X-524-68-54

PREPRINT

NASA TM X-63336

DC-BIASED PHOTOCONDUCTIVE DETECTION OF WIDEBAND CARBON DIOXIDE LASER SIGNALS

JOHN H. McELROY

FEBRUARY 1968

GSFC

GODDARD SPACE FLIGHT CENTER

GREENBELT, MARYLAND

X-524-68-54
Preprint

DC-BIASED PHOTOCONDUCTIVE DETECTION OF WIDEBAND CARBON DIOXIDE LASER SIGNALS

John H. McElroy

February 1968

GODDARD SPACE FLIGHT CENTER
Greenbelt, Maryland

DC-BIASED PHOTOCONDUCTIVE DETECTION OF WIDEBAND CARBON DIOXIDE LASER SIGNALS

John H. McElroy
Optical Systems Branch
Advanced Development Division

ABSTRACT

The application of dc-biased photoconductive detectors to the reception of wideband CO_2 laser signals is described. Signal-to-noise power ratios in the detection of AM, PM, and FM by photomixing are derived and the $(1+\omega^2\tau^2)^{-1}$ dependence of both signal and noise is shown. Expressions are given for the maximum tolerable mechanical vibration amplitude in a photomixing system and for the beam alignment requirements. Local oscillator power requirements are then discussed and it is shown that no less than 10 mw are required to assure g-r noise limited operation in a typical extrinsic germanium photoconductor. Measurement techniques are then described from which detector quantum efficiency, majority carrier lifetime, and mobility can be determined.

CONTENTS

CONTENTS (Continued)

LIST OF APPENDICES

LIST OF APPENDICES (Continued)

LIST OF FIGURES

LIST OF TABLES

DC-BIASED PHOTOCONDUCTIVE DETECTION OF WIDEBAND CARBON DIOXIDE LASER SIGNALS

Section I

INTRODUCTION

The carbon dioxide laser provides high powers with high efficiencies at 10.6 microns, a wavelength in the highly transmitting 8 to 13 micron atmospheric "window." The utilization of this laser for communication requires sensitive, wideband receivers. Photoconductive detectors suitable for use at this wavelength have been available for a number of years and are commonly found in infrared surveillance and reconnaissance equipment. Although such equipment requires highly sensitive detectors, its response time requirements are exceedingly modest by communications standards. For this reason, the available literature is slanted toward low frequency applications where response times must only rarely be less than one microsecond. If the possibilities of the carbon dioxide laser are to be exploited for communications, particularly in space communications where high Doppler frequency shifts must be tolerated, detector response times on the order of nanoseconds and even fractional nanoseconds are required.

The purpose of the following report is to examine the application of bulk photoconductive detectors, with dc bias, to the detection of wideband carbon dioxide laser signals. Because possible space communications work requires the maximum possible sensitivity, the primary emphasis of the report is placed upon the use of the photoconductor as an infrared mixer in a coherent communication system. The report is divided into eight major sections:

- An analysis of the detection of amplitude-modulated signals by photomixing
- An analysis of the detection of angle-modulated signals by photomixing
- Phase perturbation effects in AM photomixing systems
- Laser beam alignment requirements for photomixing
- Local oscillator power requirements in photomixing

- Experimental techniques for determining a detector's responsive quantum efficiency, majority carrier lifetime, and mobility
- The application of microwave mixer design techniques to infrared mixers
- A discussion of the available 10.6 micron detectors.

In addition, appendices are provided with supplementary information regarding:

- Fundamental relationships of photoconductivity
- Noise phenomena in photoconductors
- The representation of modulated optical signals
- Basic photoconductive incoherent and coherent detection techniques.

Section II

SIGNAL-TO-NOISE POWER RATIOS IN THE DETECTION OF AM SIGNALS BY INFRARED PHOTOMIXING

The following section provides signal-to-noise power ratios for heterodyne and homodyne detection of four classes of amplitude-modulated signals. The four classes to be discussed are simple amplitude modulation (AM), single-sideband amplitude modulation (AMSSB), double-sideband amplitude modulation (AMDSB), and single-sideband suppressed-carrier amplitude modulation (AMSSBSC). Each of these signals is defined and its mathematical representation given in Appendix C. Since the following discussion presupposes some understanding of photoconduction, two appendices are provided which summarize the relationships that will be employed below. Appendix A discusses the fundamental equations of photoconductivity and Appendix B lists the various noise terms that must be considered in the use of photoconductive detectors. In addition, an elementary discussion of incoherent and coherent photoconductive detection, suitable for approximate calculations, is given in Appendix D.

Simple Amplitude Modulation (AM)

Photomixing involves the combination of the incoming information signal with a local oscillator beam in a nonlinear device (see Appendix D for a further discussion). The nonlinear device, a photoconductive detector in this case, generates a difference signal, which contains the information, that may be processed in a conventional manner. The current generated by the incident photon flux may be approximated by the equation (see Appendix A)

$$i \cong \left[\epsilon^{-t/\tau} \int \frac{\eta}{\tau} P(t)\, \epsilon^{t/\tau}\, dt\right] e\, G \qquad (1)$$

where τ is the majority carrier lifetime, η is the responsive quantum efficiency, $P(t)$ is the incident photon flux, e is the electronic charge, and G is the photoconductive gain. If a simple AM signal

$$\mathcal{E}_s = E_c\,(1 + m \cos \omega_m t) \cos \omega_c t \qquad (2)$$

where E_c is the peak carrier E-field, m is the modulation index, ω_m is the modulation frequency in radians per second, and ω_c is the carrier frequency, is combined with a local oscillator signal given by

$$\mathcal{E}_L = E_L \cos(\omega_L t + \phi) \tag{3}$$

where E_L is the peak local oscillator E-field, ω_L is the local oscillator frequency, and ϕ is the phase angle of the local oscillator signal with respect to some chosen reference, the mean-squared signal current obtained from Equation (1) leads to a signal-to-noise power ratio given by

$$\left(\frac{S}{N}\right)_p = \frac{\eta \overline{P_s}}{2h\nu\Delta f}\left[1 + \frac{k(T_p + T_A)(1 + \omega_{IF}^2 \tau^2)}{eV_p G}\right]^{-1} \tag{4}$$

$\overline{P_s}$ is the average available signal power, h is Planck's constant, ν is the carrier frequency in Hertz, Δf is the system bandwidth, k is Boltzmann's constant, T_p is the photoconductor temperature, T_A is the effective input noise temperature of the succeeding amplifier, ω_{IF} is the intermediate frequency, and V_p is the average voltage across the photoconductor. The average available signal power is given by

$$\overline{P_s} = \sqrt{\frac{\epsilon}{\mu}}\,\frac{m^2 E_c^2}{4}\,. \tag{5}$$

The details of this derivation are given in Appendix E.

Repeating the procedure for a homodyne system gives

$$\left(\frac{S}{N}\right)_p = \frac{\eta \overline{P_s} \cos^2\phi}{h\nu\Delta f}\left[1 + \frac{k(T_p + T_A)(1 + \omega_m^2 \tau^2)}{eV_p G}\right]^{-1} \tag{6}$$

AMSSB

If the upper sideband of a simple AM signal is suppressed, the resulting AMSSB signal is

$$\mathcal{E}_s = E_c \cos\omega_c t + \frac{mE_c}{2}\cos\left[(\omega_c - \omega_m)t\right]. \tag{7}$$

Combining this signal with a local oscillator signal in a heterodyne system leads to a signal-to-noise power ratio again given by Equation (4) with the exception that $\overline{P_s}$ is now given by

$$\overline{P_s} = \sqrt{\frac{\epsilon}{\mu}} \frac{m^2 E_c^2}{8}. \tag{8}$$

For homodyne detection, the signal-to-noise power ratio is identical to Equation (6) with two exceptions: first, the $\cos^2 \phi$ term does not appear and, second, $\overline{P_s}$ is given by Equation (8).

AMDSB

The signal resulting from the suppression of the carrier (leaving, however, both sidebands intact) is

$$\mathcal{E}_s = mE_c \cos \omega_c t \cos \omega_m t . \tag{9}$$

In a heterodyne system, the signal-to-noise power ratio is given by Equation (4) and $\overline{P_s}$ by (5). Equation (6) applies for the homodyne system.

AMSSBSC

When both the carrier and upper sideband are suppressed, the signal is

$$\mathcal{E}_s = \frac{mE_c}{2} \cos\left[(\omega_c - \omega_m) t\right]. \tag{10}$$

Inserting this signal into a heterodyne system leads to a signal-to-noise power ratio given by Equation (4) with $\overline{P_s}$ given by (8). The homodyne case satisfies (6) without the $\cos^2 \phi$ factor and $\overline{P_s}$ is again given by (8).

Comparison of the Four AM Systems

The preceding discussion makes it obvious that each of the heterodyne and homodyne detection systems for the various modulation types is governed by a signal-to-noise power ratio of a fundamentally similar nature. There are, however, significant differences in $\overline{P_s}$ and in the required post-mixer bandwidth. Table 1 shows a comparison of the various systems. The first column lists the

Table 1

Comparison of Heterodyne and Homodyne Detection of AM Signals

Modulation Type	$(S/N)_p$	$\overline{P_s}$	Minimum Required Bandwidth	Quality Factor
AM				
Heterodyne	$\frac{\eta \overline{P_s}}{2h\nu\Delta f}$	$\sqrt{\frac{\epsilon}{\mu}} \frac{m^2 E_c^2}{4}$	$2 f_m$	¼
Homodyne	$\frac{\eta \overline{P_s}}{h\nu\Delta f} \cos^2 \phi$	$\sqrt{\frac{\epsilon}{\mu}} \frac{m^2 E_c^2}{4}$	f_m	$\cos^2 \phi$
AMSSB				
Heterodyne	$\frac{\eta \overline{P_s}}{2h\nu\Delta f}$	$\sqrt{\frac{\epsilon}{\mu}} \frac{m^2 E_c^2}{8}$	f_m	¼
Homodyne	$\frac{\eta \overline{P_s}}{h\nu\Delta f}$	$\sqrt{\frac{\epsilon}{\mu}} \frac{m^2 E_c^2}{8}$	f_m	½
AMDSB				
Heterodyne	$\frac{\eta \overline{P_s}}{2h\nu\Delta f}$	$\sqrt{\frac{\epsilon}{\mu}} \frac{m^2 E_c^2}{4}$	$2 f_m$	¼
Homodyne	$\frac{\eta \overline{P_s}}{h\nu\Delta f} \cos^2 \phi$	$\sqrt{\frac{\epsilon}{\mu}} \frac{m^2 E_c^2}{4}$	f_m	$\cos^2 \phi$
AMSSBSC				
Heterodyne	$\frac{\eta \overline{P_s}}{2h\nu\Delta f}$	$\sqrt{\frac{\epsilon}{\mu}} \frac{m^2 E_c^2}{8}$	f_m	¼
Homodyne	$\frac{\eta \overline{P_s}}{h\nu\Delta f}$	$\sqrt{\frac{\epsilon}{\mu}} \frac{m^2 E_c^2}{8}$	f_m	½

ideal signal-to-noise power ratios (neglecting the frequency dependence of these expressions). The second column gives the available signal power and the third column gives the minimum required post-mixer bandwidth in terms of the maximum modulation frequency, f_m. The final column gives a multiplicative quality parameter which shows how far short of the maximum possible signal-to-noise power ratio the given ideal ratio falls. The maximum ratio is given by

$$\left(\frac{S}{N}\right)_p = \frac{\eta\left(\sqrt{\frac{\epsilon}{\mu}}\,\frac{m^2 E_c^2}{4}\right)}{h\nu f_m} \tag{11}$$

The highest possible quality parameter is unity. As can be seen in Table 1, the AM homodyne and AMDSB homodyne systems would be optimum if ϕ can be nulled and maintained in a null condition. If ϕ must be considered random, giving $\cos^2 \phi$ an average value of one-half, the AMSSB and AMSSBSC systems would be equally effective. Due to the difficulty of reinserting a proper carrier signal at the receiver and the lack of truly satisfactory suppression techniques for 10.6 microns, the AM homodyne system would in most cases be preferred. A consideration not appearing in Table 1 concerns the large Doppler shifts that will be encountered in space applications. If a tunable local oscillator could be inserted into a heterodyne system so that the Doppler shift could be negated, a relatively narrow post-mixer bandwidth could be employed. This bandwidth would be far smaller than that which could be used with a simple homodyne system. In this manner, the simple AM heterodyne system would be the best choice.

Section III

SIGNAL-TO-NOISE POWER RATIOS IN PHOTOCONDUCTIVE DETECTION OF ANGLE-MODULATED SIGNALS

The following section considers homodyne and heterodyne detection of angle-modulated signals. Detection of narrow and wideband phase-modulated signals is first considered. A discussion of the detection of frequency-modulated signals follows.

Detection of Phase-Modulated Signals

There are two categories of phase modulation to be considered: narrow-band and wideband. The two categories are differentiated by the magnitude of the phase modulation index (see Appendix C).

First consider heterodyne detection of a narrow-band phase-modulated signal. A phase-modulated signal is represented by

$$\mathcal{E}_s = E_c \cos(\omega_c t + m_p \sin \omega_m t) \tag{12}$$

where m_p is the phase modulation index. When m_p is much less than one (narrow-band phase modulation) and the signal described by Equation (12) is combined with a local oscillator beam in a heterodyne system, the resulting signal-to-noise power ratio is

$$\left(\frac{S}{N}\right)_p = \frac{\eta \overline{P_s}}{2h\nu\Delta f}\left[1 + \frac{k(T_P + T_A)(1 + \omega_{IF}^2 \tau^2)}{eV_p G}\right]^{-1} \tag{13}$$

where

$$\overline{P_s} = 2J_1^2(m_p)\overline{P_c} \tag{14}$$

and

$$\overline{P_c} = \sqrt{\frac{\epsilon}{\mu}}\,\frac{E_c^2}{2}. \tag{15}$$

J_1 is a Bessel function of the first kind.

Similarly, the signal-to-noise power ratio for homodyne detection is

$$\left(\frac{S}{N}\right)_p = \frac{\eta \overline{P_s}}{h\nu \Delta f} \left[1 + \frac{k(T_p + T_A)(1 + \omega_m^2 \tau^2)}{eV_p G}\right]^{-1} \tag{16}$$

where it has been assumed that the signal and local oscillator beams have been locked at a relative phase difference of $\pi/2$.

If m_p is not much less than one, the phase modulation is termed wideband. Equations identical to (13) and (16) are obtained for heterodyne and homodyne detection if $\overline{P_s}$ is defined by

$$\overline{P_s} = 2 \sum_{n=1}^{N} J_n^2 (m_p) \overline{P_c} . \tag{17}$$

Detection of Frequency-Modulated Signals

The detection of frequency-modulated signals is described by equations which are nearly identical with those for phase-modulated signals. The only difference is in the value for $\overline{P_s}$. In the heterodyne system,

$$\overline{P_s} = 2 \sum_{n=1}^{N} J_n^2 (D) \overline{P_c} . \tag{18}$$

In the homodyne system, with the relative phase difference between carrier and local oscillator locked at $\pi/2$,

$$\overline{P_s} = 2 \sum_{n=1}^{N} J_n^2 (D) \overline{P_c} . \tag{19}$$

It should be noted that the upper limit on the summations in Equations (18) and (19) is N rather than infinity. This simply indicates that the series is truncated by the finite bandwidth limitations associated with any real system. The number used for N will be a characteristic of the particular system under study and must be determined within the context of that system.

Section IV

PHASE PERTURBATION EFFECTS IN AM PHOTOMIXING DETECTION SYSTEMS

In the preceding discussions it was tacitly assumed that any phase difference between the carrier and local oscillator signals in photomixing systems could be treated as a constant. In some cases it was assumed that the phase difference could be adjusted or held at a particular value. For more general situations, such an assumption may be unrealistic. Random perturbations of the phase of the signal may be induced by its passage through a turbulent medium such as the atmosphere. Another possible source of phase perturbations would be mechanical vibrations of the mirrors, or other optical components, employed in optical mixing systems. It is clear that no brief analysis could completely discuss all aspects of the effects of such perturbations in an optical communications system. For this reason, the succeeding discussion is intended to be suggestive of such effects, but certainly not definitive.

Figure 1 shows the manner in which phase perturbations might be introduced into an interferometer — either deliberately for purposes of modulation or unintentionally due to mechanical instabilities of the interferometer structure.

In order to analyze the effects of phase perturbations, an idealized situation will be examined. It will be assumed that the signal to be detected is a simple AM signal with a single modulation frequency. It will be further assumed that the phase perturbation introduced into the system is a single frequency sinusoid. The extension to somewhat more complicated cases via Fourier techniques will be obvious.

To account for phase perturbations, let the local oscillator signal be given by

$$\mathcal{E}_L = E_L \cos(\omega_L t + \alpha \sin \omega_p t) \tag{20}$$

where ω_p is the perturbation frequency and α is the peak amplitude of the perturbation. For illustration, consider a homodyne system. Combining the local oscillator with the simple AM signal gives a time-averaged, mean-squared, resultant E-field at the detector given by

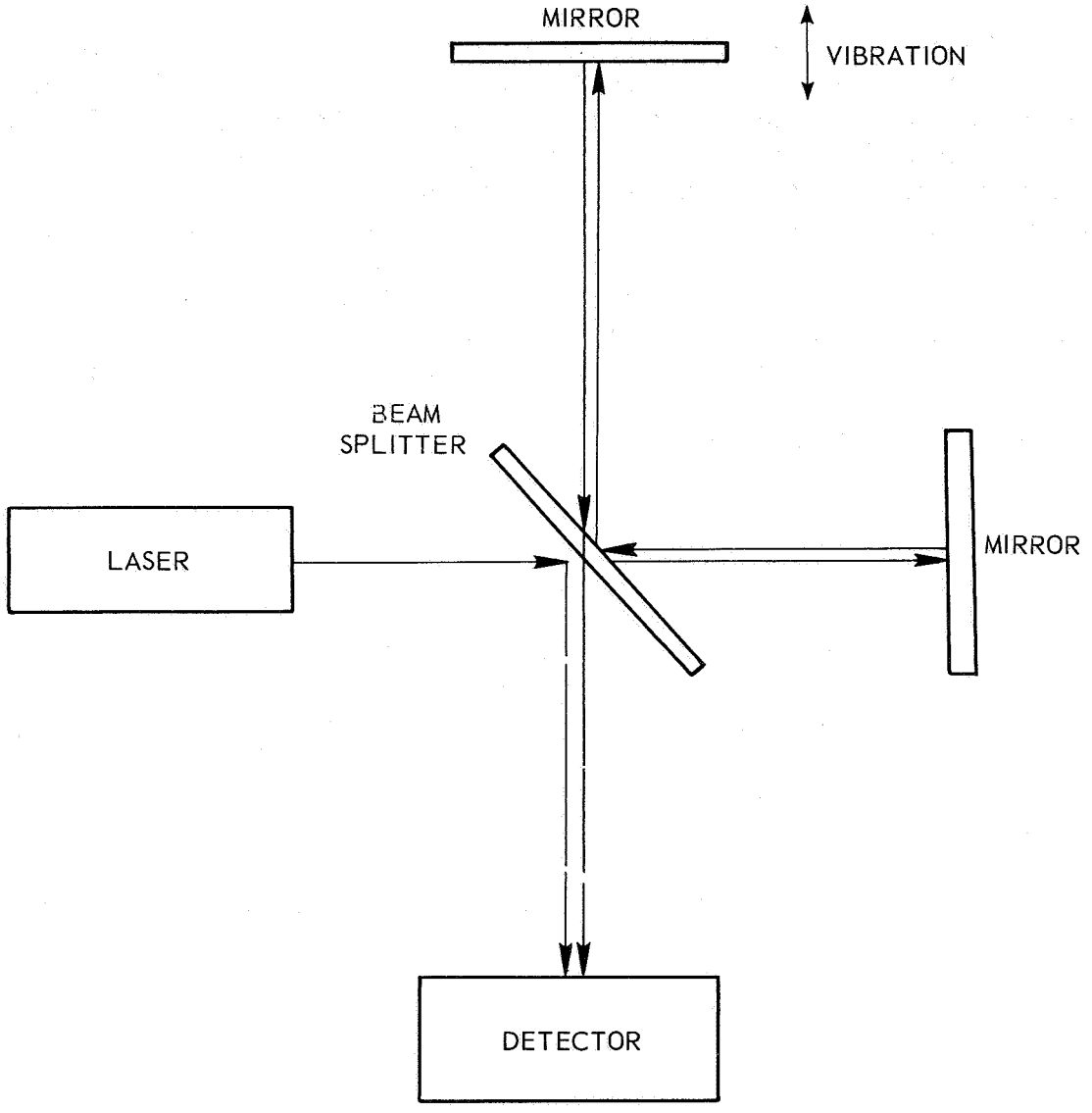

Figure 1. Optical Homodyne System Employing a Michelson Interferometer

$$\overline{\mathcal{E}_R^2} \cong \frac{E_L^2}{2} + E_L E_c (1 + m \cos \omega_m t) \left[J_0(\alpha) + 2 \sum_{n=1}^{N} J_n(\alpha) \cos (n\omega_p t) \right]. \quad (21)$$

Therefore, employing Equation (1), the resulting signal current is

$$i = \frac{e \eta G}{h \nu} \sqrt{\frac{\epsilon}{\mu}} \left[\frac{E_L^2}{2} + E_L E_c J_0(\alpha) + m E_L E_c J_0(\alpha) \frac{\cos (\omega_m t + \phi_1)}{\sqrt{1 + (\omega_m \tau)^2}} \right]$$

$$+ \frac{e \eta G}{h \nu} \sqrt{\frac{\epsilon}{\mu}} E_L E_c \sum_{n=1}^{N} J_n(\alpha) \left\{ \frac{2 \cos (n\omega_p t + \phi_2)}{\sqrt{1 + (n\omega_p \tau)^2}} \right.$$

$$\left. + \frac{m \cos \left[(\omega_m + n\omega_p) t + \phi_3 \right]}{\sqrt{1 + (\omega_m + n\omega_p)^2 \tau^2}} + \frac{m \cos \left[(\omega_m - n\omega_p) t + \phi_4 \right]}{\sqrt{1 + (\omega_m - n\omega_p)^2 \tau^2}} \right\} \quad (22)$$

where

$$\phi_1 = \tan^{-1} (-\omega_m \tau),$$

$$\phi_2 = \tan^{-1} (-n\omega_p \tau),$$

$$\phi_3 = \tan^{-1} -\left[(\omega_m + n\omega_p) \tau \right],$$

and

$$\phi_4 = \tan^{-1} -\left[(\omega_m - n\omega_p) \tau \right].$$

The spectrum of the signal is shown in Figure 2.

Equation (22) shows that the phase perturbation places sidebands about the modulation frequency and introduces low frequency components at multiples of the perturbation frequency. It may also be deduced that, if a number of modulation frequencies are involved, sidebands would be produced about each modulation frequency. The presence of so many additional frequency components can substantially degrade the performance of a detection system.

The above discussion can be used to place maximum bounds on the amplitude of mechanical vibrations which may be present in an interferometer. This is of particular interest where a homodyne receiver is to be mounted on a servo-driven telescope. The servosystem may produce vibrations which could be coupled through the mounting structure into the receiver. It can be seen that the problem may be reduced to making the frequency components at $\omega_m \pm \omega_p$ negligible with respect to the amplitude of the desired signal. Therefore, the required condition is

$$| J_0(\alpha) | >> | J_1(\alpha) |$$

For illustration, assume that if $J_0(\alpha)$ is 10 times greater than $J_1(\alpha)$ sufficient discrimination is obtained. Further assume that a CO_2 laser system operating at 10.6 microns is being used in the system under study. Examining a table of Bessel functions leads to the conclusion that $\alpha \leq 0.2$ radian satisfies the required condition. In a system such as that shown in Figure 1, the bound on α requires that the mirrors be stable within nominally 0.2 micron.

It is also of interest to determine the value of α for which the amplitude of the extraneous signal is equal to that of the desired signal. Again examining a table of Bessel functions, it is found that an α of 1.4 radian is sufficient. In the system of Figure 1, this corresponds to a peak mechanical vibration amplitude of nominally 1.2 microns.

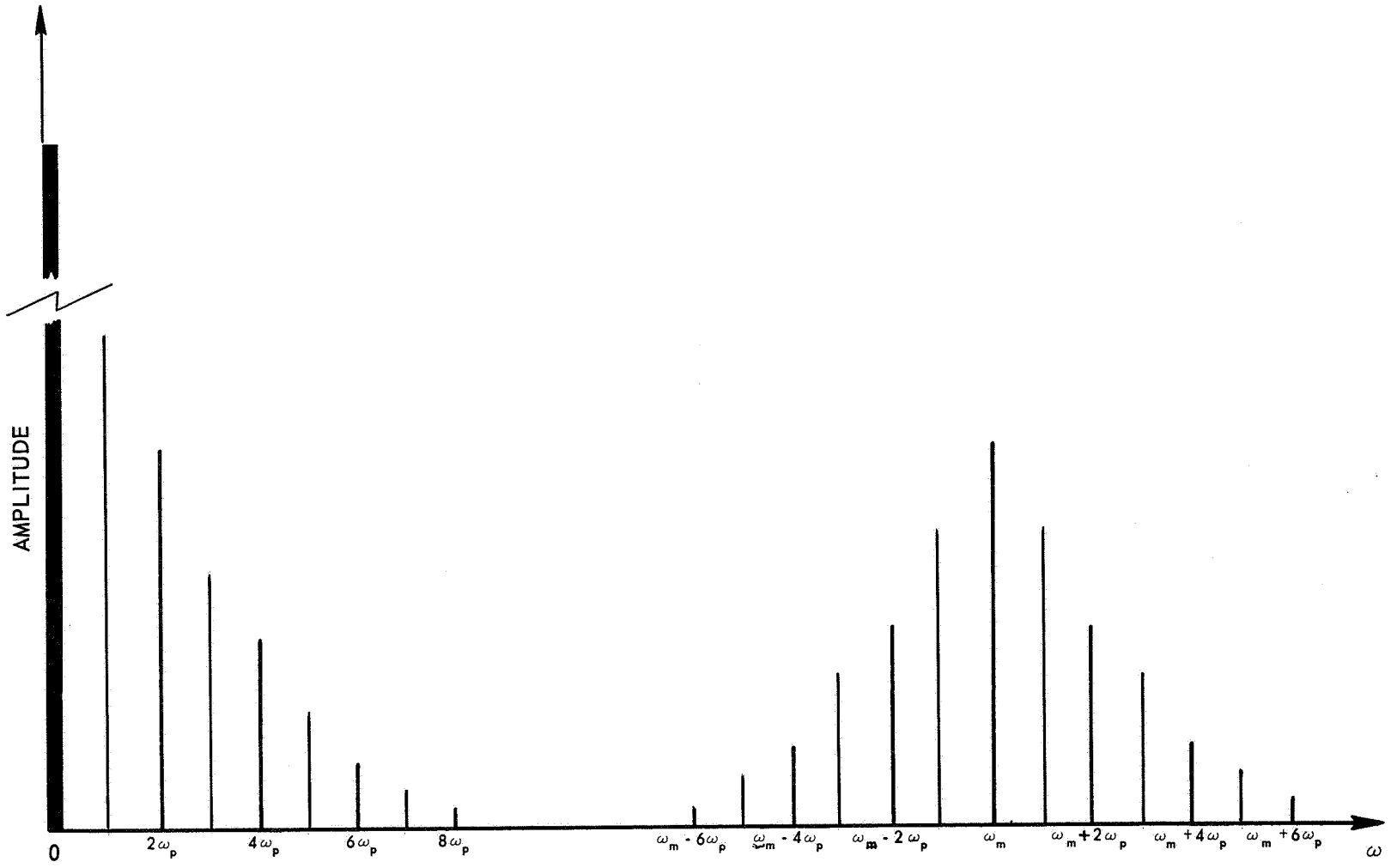

Figure 2. Frequency Spectrum of Homodyne Detected Phase Perturbed AM Signal

Section V

BEAM ALIGNMENT REQUIREMENTS IN PHOTOMIXING SYSTEMS

In homodyne and heterodyne detection systems the signal and local oscillator beams must be aligned in two respects: polarization and direction of propagation. Each requirement will be considered separately below. The problem is diagrammed in Figure 3.

Polarization Alignment Requirements

Consider the case of a signal and local oscillator beam whose polarizations differ by an angle θ, but whose directions of propagation agree perfectly. The mean-squared resultant E-field is

$$\overline{\mathcal{E}_R^2} = \overline{\mathcal{E}_L^2} + \overline{\mathcal{E}_s^2} + \overline{2\,\mathcal{E}_L\,\mathcal{E}_s \cos\theta} \tag{23}$$

Since the third term contains the signal information, it is seen that the signal produced by the photoconductor will vary directly as the cosine of the angular difference in polarization. Therefore, orthogonally polarized beams will produce no beat signal.

A tacit assumption made above is that the detector element is not itself polarization sensitive. It has been observed in mixing experiments involving photoelectric emission that mixing can occur between orthogonally polarized light beams (see Reference 1). This is due to the vectorial photoelectric effect resulting from dependence of the quantum efficiency of the photoelectric surface upon polarization. No such effect has been reported in bulk photoconductors.

Direction of Propagation Alignment Requirements

It will now be assumed that the signal and local oscillator beams are aligned in polarization. It will be further assumed that the directions of propagation of the two beams are misaligned by an angle ψ. Ross (see Reference 2) has shown that the photoinduced current in the photoconductor is proportional to

$$i \sim \overline{\mathcal{E}_L^2} + \overline{\mathcal{E}_s^2} + E_L\,E_c \cos\omega_{IF}\,t\,\frac{\sin\left(\dfrac{\pi D \sin\psi}{\lambda_{LO}}\right)}{\dfrac{\pi D \sin\psi}{\lambda_{LO}}} \tag{24}$$

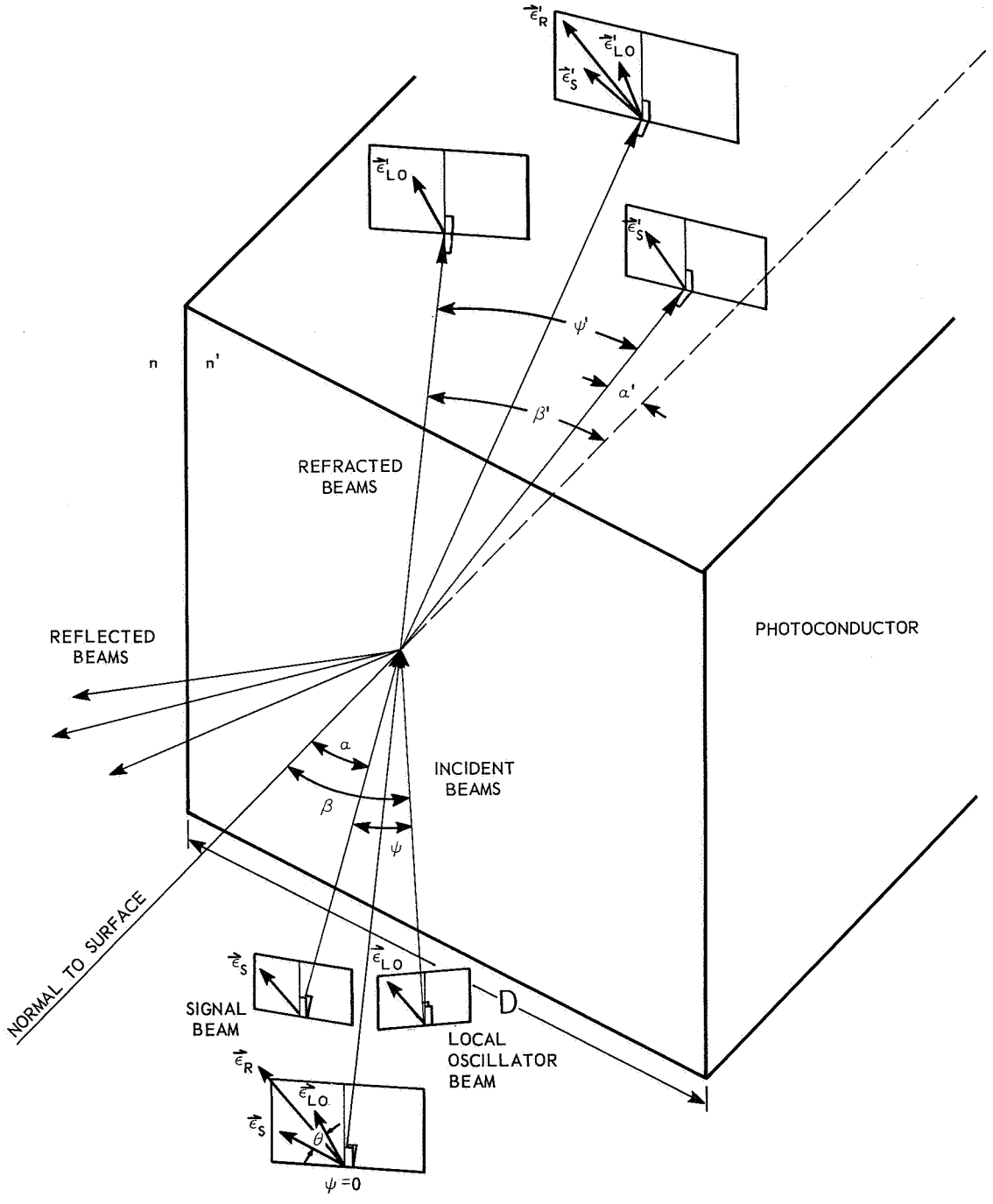

Figure 3. Diagram Depicting Alignment Requirements Associated with Photomixing

where D is shown in Figure 3 and λ_{LO} is the local oscillator wavelength. For the 10.6 micron radiation from a CO_2 laser and a detector for which D is one millimeter, the desired signal current varies as

$$i_s \sim E_L E_s \cos \omega_{IF} t \frac{\sin (3 \times 10^3 \sin \psi)}{3 \times 10^3 \sin \psi} \tag{25}$$

Therefore, the signal current will be reduced by less than 10 percent if

$$3 \times 10^2 \sin \psi \leq 0.75$$

This places a bound on ψ such that the two beams must be aligned within nominally ten minutes of arc.

Siegman (see Reference 3) has given an alternative analysis from the point of view of antenna theory that should be examined by the reader wishing to pursue these matters further.

Section VI

LOCAL OSCILLATOR POWER REQUIREMENTS

The determination of the required local oscillator power is influenced primarily by two factors: first, the requirement to achieve G-R noise limited operation and, second, the requirement to match the detector impedance to the input impedance of the preamplifier following the detector.

Achieving G-R Noise Limited Operation

The requirement to achieve G-R noise limited operation is satisfied by ensuring that the G-R noise produced by the local oscillator exceeds the Johnson, low-frequency, background, and amplifier noise terms. For sake of illustration, assume that the background and low-frequency noise terms are less than the Johnson and amplifier noise terms, as would ordinarily be the case. Under this assumption, the required condition is that

$$\frac{4\, e^2\, \frac{\eta\, G^2}{h\nu}\, \Delta f\, \overline{P_{LO}}}{1 + \omega_{IF}^2\, \tau^2} \gg \frac{4\, k\, (T_p + T_A)\, \Delta f}{R_p} . \tag{26}$$

Assuming that the bias voltage has been optimized, the load and photoconductor resistance have been matched, that $T_A \gg T_p$, and that $\omega_{IF}^2\, \tau^2 \ll 1$ Equation (26) reduces to

$$\overline{P_{LO}} \gg \frac{k\, T_A\, h\nu}{\eta\, e^2\, G^2\, R_p} . \tag{27}$$

Substituting typical values (see Reference 4) into Equation (27) for a 10.6 micron detection system ($T_A = 1160°K$, $\nu \cong 3 \times 10^{13}$ Hz, $\eta = 0.15$, $\tau = 10^{-9}$ sec, $T_r = 1.25 \times 10^{-9}$ sec, and $R_p = 200$ ohms) it is found that the local oscillator power must be greater than nominally 8.7 milliwatts.

Effect of Local Oscillator Power on Mixer IF Output Resistance

Since the local oscillator flux is the dominant force controlling the conductivity of a photoconductive mixer, it may be employed to adjust the resistance of the photoconductor to an optimum value for impedance matching to the preamplifier.

In general, wide bandwidth systems require low mixer resistances. Under normal circumstances a photoconductive detector has a high resistance (500K ohms to 1 M ohm). Therefore, the local oscillator is used to drastically lower the mixer resistance. For extrinsic photoconductors, however, it is necessary that the local oscillator power not be increased to the point where it totally exhausts the dopant energy levels.

To relate the local oscillator power to the resistance of the photoconductor, note that the dc photocurrent can be written as

$$I_o = \frac{e \eta \overline{P_{LO}}}{h \nu} G \tag{28}$$

Therefore, the IF output resistance under matched conditions is given by

$$R_o = \frac{h \nu V_p}{e \eta G \overline{P_{LO}}} \tag{29}$$

The bias voltage and local oscillator power may then be selected in accordance with this equation to obtain the desired output resistance.

Section VII

DETERMINATION OF DETECTOR QUANTUM EFFICIENCY, MAJORITY CARRIER LIFETIME, AND MOBILITY

The equations presented in the preceding sections require a knowledge of the photoconductive gain, quantum efficiency, majority carrier lifetime, and mobility. Since the photoconductive gain is determined by the mobility and carrier lifetime through the relationship

$$G = \frac{\tau}{T_r} = \frac{\tau \mu V_p}{L^2} \tag{30}$$

where L is the interelectrode spacing, the list of required parameters can be reduced to the last three named. The labels assigned to the various dimensions of a photoconductor, to which reference will be made in the succeeding discussion, are shown in Figure 4.

In general, none of the three parameters will be known to the experimenter. The next three subsections discuss simple measurements from which the quantum efficiency, majority carrier lifetime, and carrier mobility may be deduced to a moderate degree of accuracy.

Quantum Efficiency

The responsive quantum efficiency, the ratio of the number of current carriers generated by the signal radiation striking the detector to the number of photons in the signal radiation, can be determined by very simple measurements. Assume that the photoconductor is connected to the circuit shown in Figure 5.

The responsive quantum efficiency is obtained by measuring the change in the output voltage for a change in the signal photon flux. If ΔV_s represents the change in the output voltage and ΔP_s is the change in the signal photon flux responsible for the change in voltage, the responsive quantum efficiency is given by

$$\eta = \frac{\Delta V_s / e R_L}{\Delta P_s / h\nu} = \frac{h\nu}{e R_L} \frac{\Delta V_s}{\Delta P_s} . \tag{31}$$

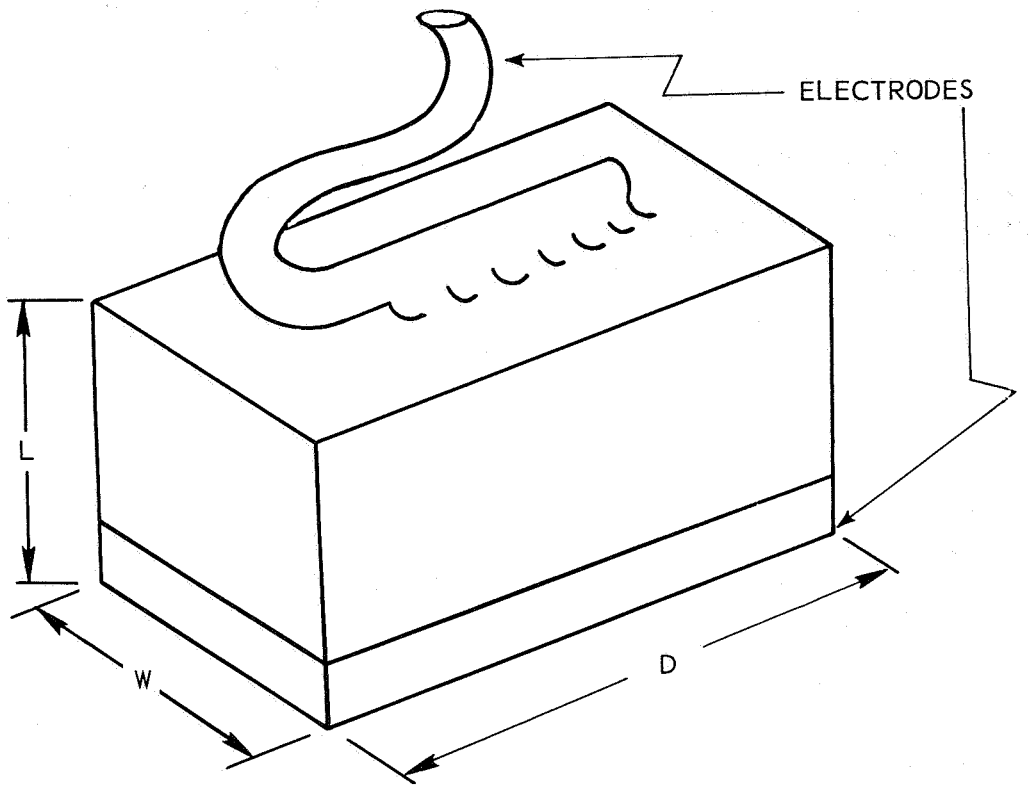

Figure 4. Photoconductor Dimensions

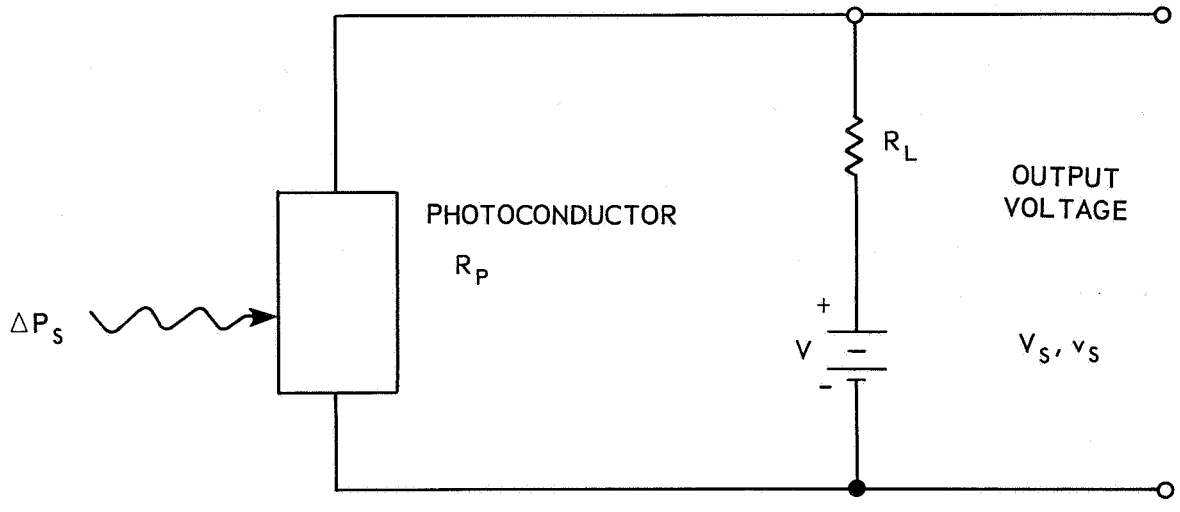

Figure 5. Circuit for Determining Responsive Quantum Efficiency

Majority Carrier Lifetime

In the following discussion it will be assumed that the capacitance of the detector has been reduced to a small value such that any "roll-off" in frequency response may be attributed to the majority carrier lifetime. With the above assumption, two approaches may be taken to the determination of the majority carrier lifetime. One approach is the direct measurement of the response of the detector to a sufficiently rapid change in the incident photon flux. This is based upon the $(1 + \omega^2\tau^2)^{-1}$ dependence of the photoconductive response, where ω is the highest frequency contained in the change.

The generation of the nanosecond and fractional nanosecond changes in the photon flux which are necessary to evaluate detectors for gigahertz frequency capability is a difficult process at best. A number of techniques have been employed. Reflections from high-speed spinning mirrors have been used to generate light pulses having rise times on the order of one nanosecond (see Reference 5). This technique is not commonly used because of the extremely high speeds at which the mirrors must turn.

Alternatively, a laser beam may be passed through an electro-optic modulator and amplitude modulated at rates up to a nominal 150 MHz. By varying the modulation frequency up to this value, lifetimes on the order of one nanosecond can be determined (see Reference 6). The relationship

$$\tau = \frac{1}{2\pi f_o}, \tag{32}$$

where f_o is the half-power frequency (3 db point on the frequency roll-off), is used to determine the majority carrier lifetime. A diagram of such an arrangement is shown in Figure 6. The receiver in that diagram may be a tuned r-f voltmeter, spectrum analyzer, or similar device. The signal generator and attenuator are used for calibration. A similar arrangement may also be used with an acousto-optical modulator (see Reference 6).

A third technique can be employed if stable, frequency-tunable lasers are available. Such lasers are available at 3.39 microns and have been used in an experimental arrangement shown in Figure 7. The two lasers are tuned to different frequencies and heterodyned to produce a signal at the difference frequency. The signal from the test detector is compared with that from a reference detector. This procedure is predicated upon the availability of a reference detector with known frequency response characteristics and the applicability of a lifetime measurement made at 3.39 microns to the 10.6 micron wavelength.

Instead of the direct techniques described above, a second approach, relying on an indirect technique, may be used. This approach is based upon the $(1 + \omega^2\tau^2)^{-1}$

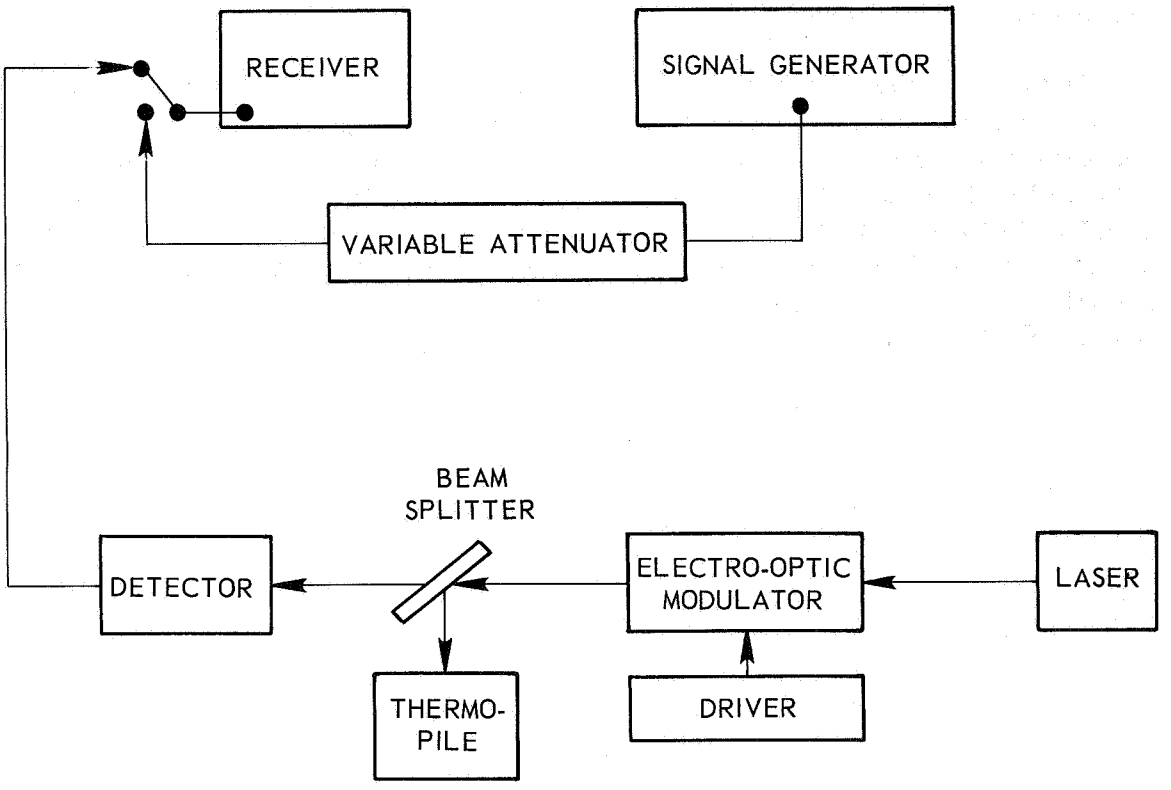

Figure 6. Electro-Optic Technique for Evaluation of Carrier Lifetime

dependence of the detector generation-recombination noise [see Equation (C4)]. It has the advantage of not requiring the generation of precise nanosecond changes in a photon stream, tunable lasers, or a reference detector. The experimental arrangement used in this approach is shown in Figure 8 and sample results in Figure 9 (see Reference 4). The G-R noise power is plotted as a function of frequency.

Majority Carrier Mobility

The following discussion, which describes a technique for determining carrier mobility, assumes that the responsive quantum efficiency and majority carrier lifetime are known. The circuit shown in Figure 5 will again be employed in the discussion below. If it is assumed that the photon flux is varied between two values by an amount ΔP_s, resulting in a change in output voltage ΔV_s, and it is further assumed that the change in photon flux is small, the majority carrier mobility can be adequately approximated by the relationship

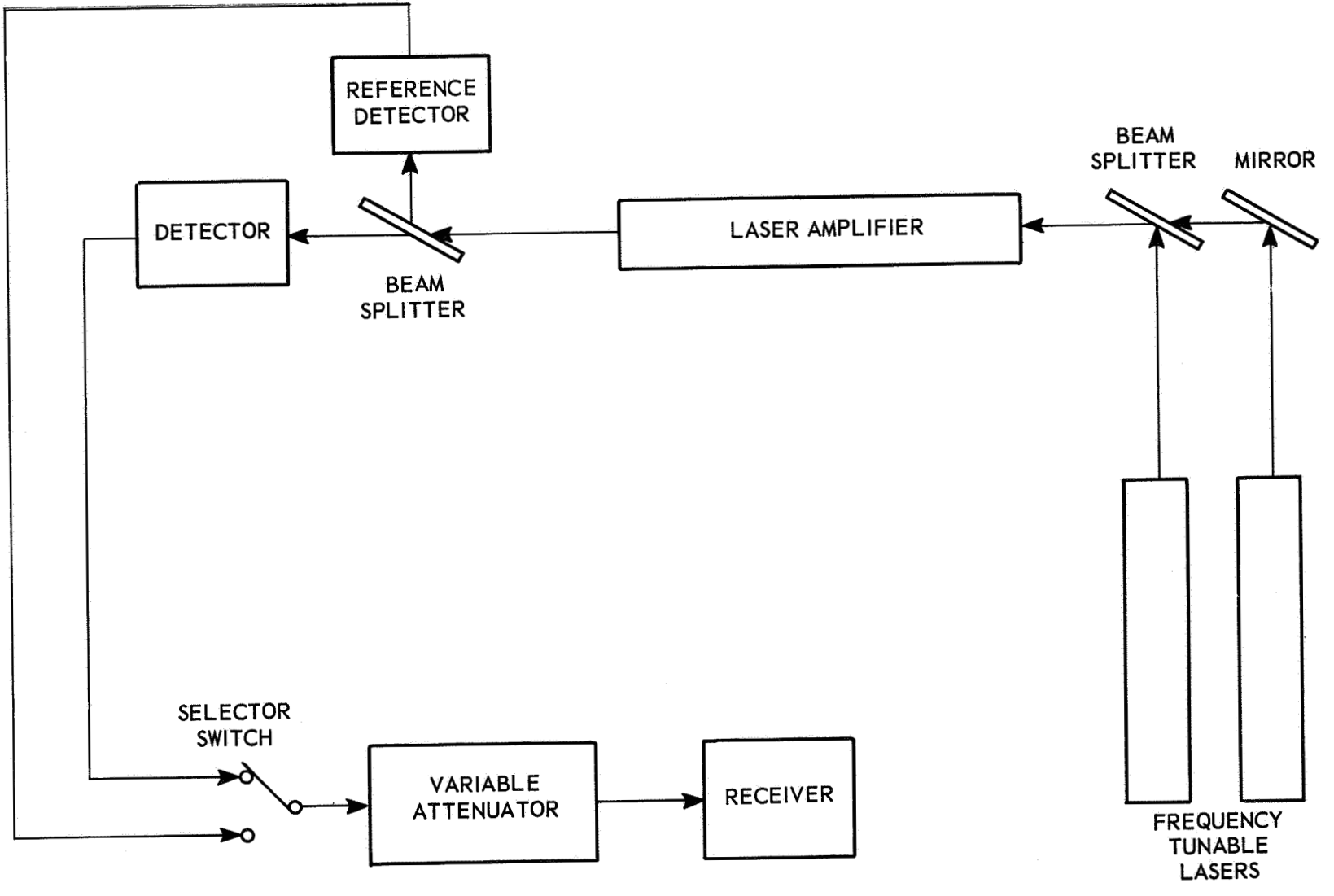

Figure 7. Heterodyne Majority Carrier Lifetime Measurement Technique

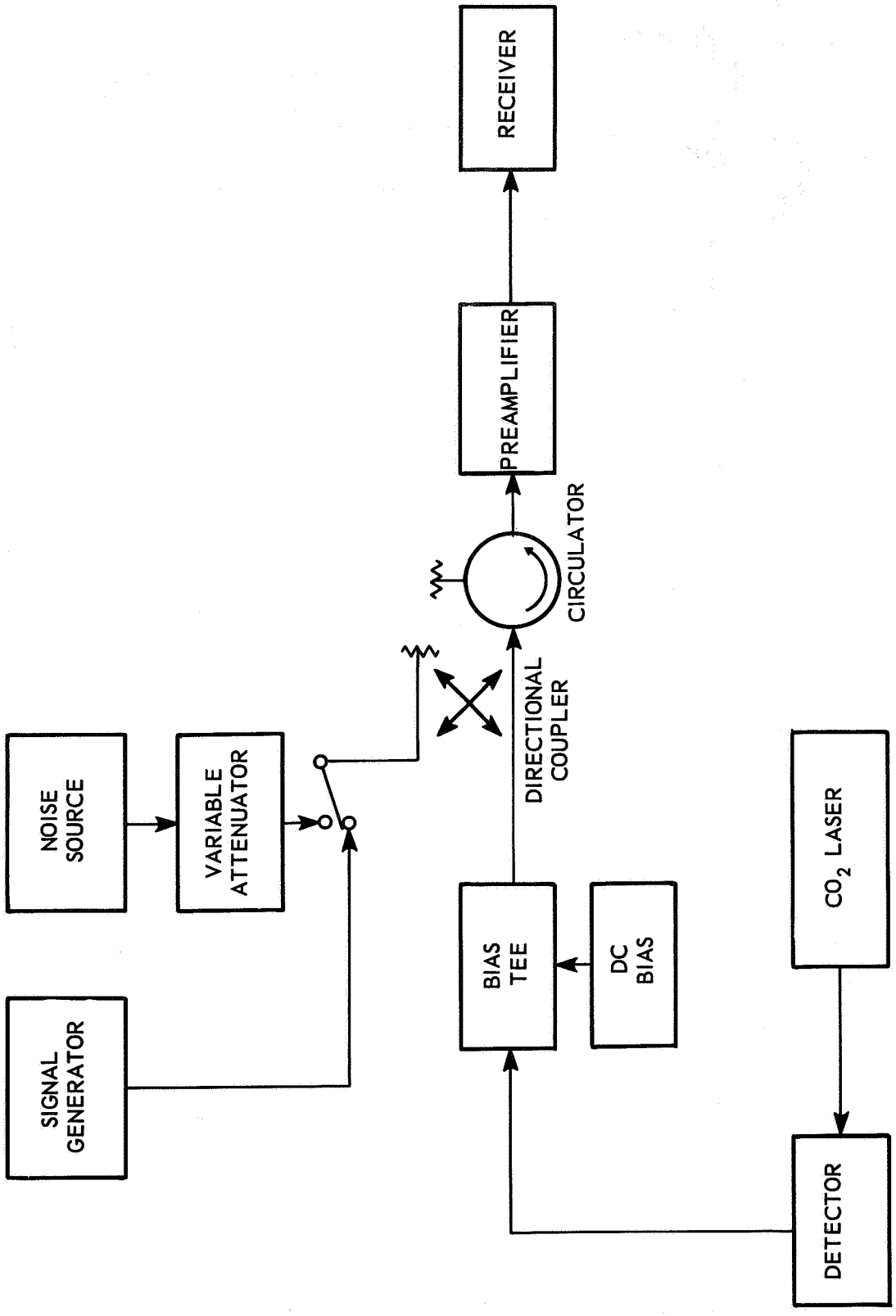

Figure 8. Experimental Setup for Lifetime Determination from G-R Noise Spectrum

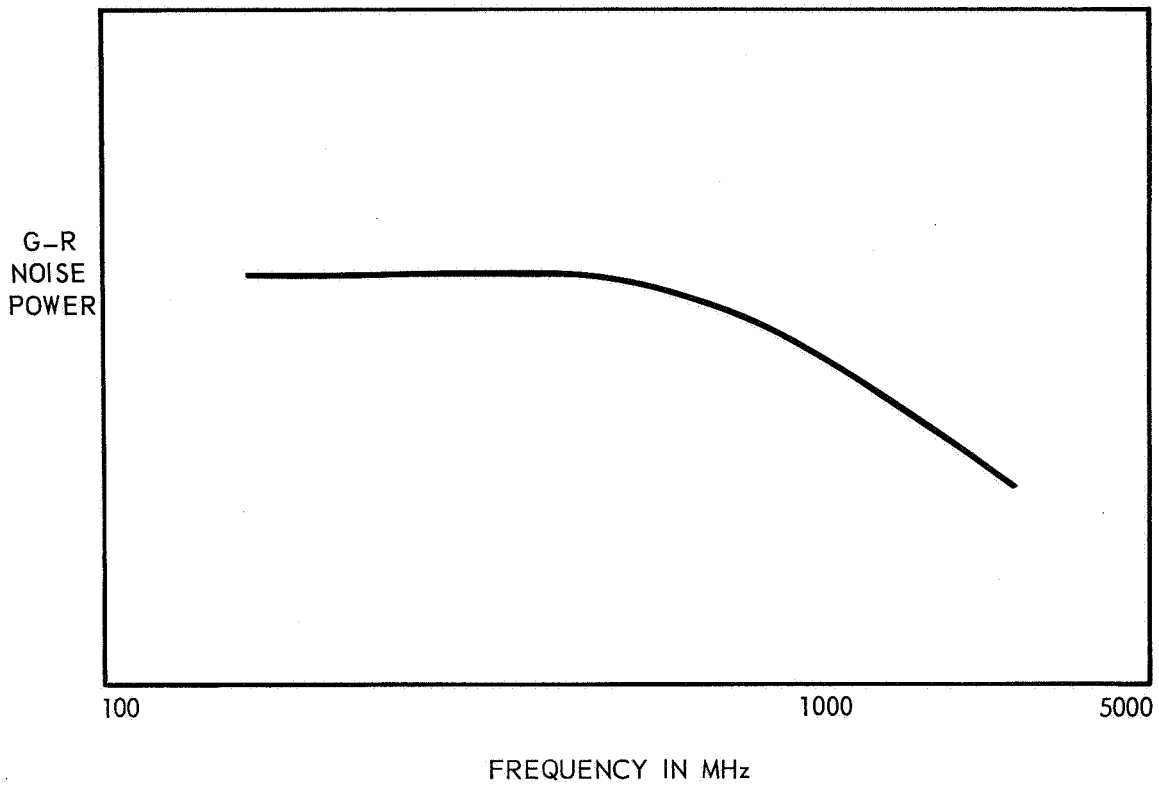

Figure 9. G-R Noise Power as a Function of Frequency

$$\mu = \frac{L\,(R_L + R_p)^2\,h\nu}{R_L\,R_p^2\,V\,e\,D\,W\,\eta\,\tau}\,\frac{\Delta V_s}{\Delta P_s} \tag{33}$$

Each term in (33) is a known or measurable quantity. A detailed derivation of this equation is given in Appendix F.

Section VIII

APPLICATION OF MICROWAVE MIXER DESIGN TECHNIQUES TO INFRARED MIXERS

Two design parameters which are popular in microwave mixer design are conversion gain (or loss) and noise factor. Related parameters can be defined for the infrared mixer (see Reference 4). Conversion gain or loss is a measure of the efficiency with which the available input signal is converted to available intermediate frequency signal power. Assuming a matched load resistance, the conversion gain for an infrared mixer employed in an AM heterodyne system is given by

$$A_c = \frac{\frac{1}{2}\,\overline{i_s^2}\,R_o}{P_s}$$

$$= \frac{e\,\eta\,G\,V_p}{h\,\nu}\,(1 + \omega_{IF}^2\,\tau^2)^{-1} \tag{34}$$

where $\overline{i_s^2}$ is given by Equation (E10) and R_o by (29). This expression clearly shows the degradation in conversion efficiency at high frequencies.

An alternative expression may be written in terms of the bias and local oscillator powers supplied to the mixer. The bias power is

$$P_b = \left(\frac{e\,\eta\,G\,P_{LO}}{h\,\nu}\right)^2 \left(\frac{h\,\nu\,V_p}{e\,\eta\,G\,P_{LO}}\right)$$

$$= \frac{e\,\eta\,G\,V_p\,P_{LO}}{h\,\nu} \tag{35}$$

Therefore,

$$A_c = \frac{P_b}{P_{LO}}\,(1 + \omega_{IF}^2\,\tau^2)^{-1} \tag{36}$$

A quantum noise factor, analogous to the microwave noise factor, can be defined to compare the mixer performance to that of a theoretical optimum mixer. The starting point for the definition is the noise equivalent power (NEP), the amount of signal power needed to obtain a unity signal-to-noise power ratio. For the simple AM case, the signal-to-noise power ratio is given by Equation (4). Equating this equation to unity and substituting for the mixer conversion gain,

$$\text{NEP} = \frac{2 h \nu \Delta f}{\eta} + \frac{2 \Delta f k (T_p + T_A)}{A_c} \tag{37}$$

The quantum noise factor, QNF, is the NEP normalized to the quantum noise, $h\nu\Delta f$. Therefore,

$$\text{QNF} = \frac{2}{\eta} + \frac{2 k (T_p + T_A)}{h \nu A_c} \tag{38}$$

The two parameters defined above serve as useful measures of the effectiveness of an infrared mixer.

Section IX

PHOTOCONDUCTIVE DETECTORS AVAILABLE FOR USE AT 10.6 MICRONS

Four materials dominate photoconductive detection at 10.6 microns: copper-doped germanium (Ge:Cu), mercury-doped germanium (Ge:Hg), mercury cadmium telluride ($Hg_{1-x}Cd_xTe$), and gold-doped germanium (Ge:Au). The first three named are suitable for actual communications work, while the fourth is primarily a convenient laboratory tool. The major characteristics of these detectors are briefly discussed in the following paragraphs.

Detectors constructed from Ge:Cu are usable in the 2 to 30 micron region. They typically have an NEP in direct detection on the order of 10^{-12} watts/$Hz^{1/2}$. In heterodyne detection an NEP of 1.3×10^{-19} watts/$Hz^{1/2}$ has been reported (see Reference 7). Response times, which are a function of the amount of compensating impurities which are added to the photoconductor, range from several nanoseconds to fractional nanosecond values (see References 6, 7, and 8). The major disadvantage of the Ge:Cu detector is its requirement to be cooled to liquid helium temperature (4.2°K).

Detectors using Ge:Hg are essentially similar to Ge:Cu detectors in their response to 10.6 micron radiation. While Ge:Hg detectors are restricted to the range 2 to 15 microns and only require cooling to 20°K, their frequency response and detectivity are in the same range as the values given above for Ge:Cu (see References 6, 9, 10, and 11).

$Hg_{1-x}Cd_xTe$ detectors are just becoming available at the time of this report and an extremely wide range of parameter values are being reported (see References 6, 9, 12, and 13). It is expected that these detectors will become available with sensitivities approaching those of Ge:Cu and Ge:Hg and sufficient frequency response to detect modulation frequencies approaching 100 MHz or greater. The significant advantage of these detectors is their considerably higher operating temperature; they require cooling only to 110°K.

Ge:Au detectors are intended for use in the 2 to 8 micron region, but find frequent laboratory use at 10.6 microns because their relative economy and high operating temperature (77°K) compensates for their lack of sensitivity. Ge:Au detectors are nominally 200 times less sensitive than Ge:Hg detectors at 10.6 microns. The response time of a Ge:Au detector can be as small as 1.5 nanoseconds (see Reference 9).

REFERENCES

1. Bahr, A. J.: The Effect of Polarization Selectivity on Optical Mixing in Photoelectric Surfaces. Proc. IEEE, Vol. 53, No. 5, May 1965, P. 513

2. Ross, M.: Laser Receivers. John Wiley & Sons, Inc., 1966

3. Siegman, A. E.: The Antenna Properties of Optical Heterodyne Receivers. Applied Optics, Vol. 5, No. 10, Oct. 1966, pp. 1588-1594

4. Arams, F. R., Sard, E. W., Peyton, B. J., and Pace, F. P.: Infrared 10.6-Micron Heterodyne Detection with Gigahertz IF Capability. Airborne Instruments Laboratory Technical Memorandum No. 58, July 1967

5. Wolfe, W. L.: Handbook of Military Infrared Technology. Office of Naval Research. Dept. of the Navy. Washington, D. C. 1965

6. Picus, G. S.: Far Infrared Laser Receiver Investigation. Interim Technical Report No. 3, 1 Sept. 1966 through 30 Nov. 1966. DDC Document AD 810764

7. Teich, M. C., Keyes, R. J., and Kingston, T. H.: Optimum Heterodyne Detection at 10.6 Microns in Photoconductive Ge:Cu. Appl. Phys. Letters, Vol. 9, No. 10, 15 Nov 1966, pp. 357-360

8. Yardley, J. T., and Moore, D. B.: Response Times of Ge:Cu Infrared Detectors. Appl. Phys. Letters, Vol. 7, No. 11, 1 Dec. 1965, pp. 311-312

9. Picus, G. S., and Buczek, C.: Far Infrared Laser Receiver Investigation. Interim Technical Report No. 4, 15 Feb. 1967 through 15 May 1967. DDC Document AD 816145

10. Buczek, C., and Picus, G. S.: Heterodyne Performance of Mercury Doped Germanium. Appl. Phys. Letters, Vol. 11, No. 5, 15 Aug. 1967, pp. 125-126

11. Aranovich, R. M., Pyatnitskii, A. I., and Karashev, T. B.: Photoelectric Properties of Mercury-Doped Germanium. Soviet Physics — Semiconductors, Vol. 1, No. 4, Oct. 1967, pp. 502-504

12. Kruse, P. W.: Photon Effects in $Hg_{1-x}Cd_xTe$. Applied Optics, Vol. 4, No. 6, June 1965, pp. 687-692

13. Verie, C., and Ayas, J.: $Cd_xHg_{1-x}Te$ Infrared Photovoltaic Detectors. Appl. Phys. Letters, Vol. 10, No. 9, 1 May 1967, pp. 241-243

BIBLIOGRAPHY

1. Abramowitz, M., and Stegun, I. A.: Handbook of Mathematical Functions. National Bureau of Standards Applied Mathematics Series. Vol. 55. U. S. Government Printing Office, March 1965

2. Anderson, L. K., and McMurtry, B. J.: High-Speed Photodetectors. Applied Optics, Vol. 5, No. 10, Oct. 1966, pp. 1573-1587

3. Arams, F. R., Sard, E. W., Peyton, B. J., and Pace, F. P.: Infrared 10.6-Micron Heterodyne Detection with Gigahertz IF Capability. Airborne Instruments Laboratory Technical Memorandum No. 58, July 1967

4. Arams, F. R., Sard, E. W., Peyton, B. J., and Pace, F. P.: Infrared 10.6-Micron Heterodyne Detection with Gigahertz IF Capability. IEEE J. Quantum Electronics, Vol. QE-3, Nov. 1967, pp. 484-492

5. Aranovich, R. M., Pyatnitskii, A. I., and Karashev, T. B.: Photoelectric Properties of Mercury-Doped Germanium. Soviet Physics — Semiconductors, Vol. 1, No. 4, Oct. 1967, pp. 502-504

6. Azaroff, L. V., and Brophy, J. J.: Electronic Processes in Materials. McGraw-Hill Book Co., Inc., 1963

7. Bahr, A. J.: The Effect of Polarization Selectivity on Optical Mixing in Photoelectric Surfaces. Proc. IEEE, Vol. 53, No. 5, May 1965, P. 513

8. Beam, W. R.: Electronics of Solids. McGraw-Hill Book Co., Inc., 1965

9. Black, H. S.: Modulation Theory. D. Van Nostrand Co., Inc., 1953

10. Bube, R. H.: Photoconductivity of Solids. John Wiley & Sons, Inc., 1960

11. Buczek, C., and Picus, G. S.: Heterodyne Performance of Mercury-Doped Germanium. Appl. Phys. Letters, Vol. 11, No. 5, 15 Aug. 1967, pp. 125-126

12. Clarke, K. K., Pickholtz, R. L., and Schilling, D. L.: A Space Communications Study. Final Report on NASA Grant NGR-33-006-020. Polytechnic Institute of Brooklyn, Sept. 15, 1966

13. Coleman, P. D., Eden, R. C., and Weaver, J. N.: Mixing and Detection of Coherent Light in a Bulk Photoconductor. IEEE Trans. on Electron Devices, Vol. ED-11, No. 11, Nov. 1964, pp. 488-497

14. Corcoran, V. J.: Directional Characteristics in Optical Heterodyne Detection Processes. J. Appl. Physics, Vol. 36, No. 6, June 1965, pp. 1819-1825

15. DeVore, H. B.: Spectral Distribution of Photoconductivity. Phys. Review, Vol. 102, No. 4, Apr. 1956, pp. 86-91

16. DiDomenico, M.: Direct Demodulation and Frequency Conversion of Microwave-Modulated Light in a CdSe Bulk Photoconductor. J. Appl. Physics, Vol. 35, No. 4, Apr. 1964, pp 1353-1354

17. DiDomenico, M., and Anderson, L. K.: Microwave Signal-to-Noise Performance of CdSe Bulk Photoconductive Detectors. Proc. IEEE, Vol. 52, No. 7, July 1964, pp 815-822

18. DiDomenico, M., and Svelto, O.: Solid-State Photodetection: A Comparison Between Photodiodes and Photoconductors. Proc. IEEE, Vol. 52, No. 2, Feb. 1964, pp. 136-144

19. Fuls, E. N.: Optical Frequency Mixing in Photoconductive InSb. Appl. Phys. Letters, Vol. 4, No. 1, 1 Jan. 1964, pp. 7-8

20. Goldman, S.: Frequency Analysis, Modulation, and Noise. McGraw-Hill Book Co., Inc., 1948

21. Goodman, J. W.: Comparative Performance of Optical-Radar Detection Techniques. IEEE Trans. on Aerospace and Electronic Systems, Vol. AES-2, No. 5, Sept. 1966, pp. 526-535

22. Hause, H. A., and Townes, C. H.: Comments on "Noise in Photoelectric Mixing." Proc. IRE, Vol. 50, No. 6, June 1962, pp. 1544-1546

23. Hunter, L. P.: Handbook of Semiconductor Electronics. McGraw-Hill Book Co., Inc., 1962

24. Jacobs, S. F.: Heterodyne Detection in Optical Communication. Final Report RADC Contract No. AF 30(602)-3591. CSFTI Document No. AD 603622. July, 1964

25. Kruse, P. W.: Photon Effects in $Hg_{1-x}Cd_xTe$. Applied Optics, Vol. 4, No. 6, June 1965, pp. 687-692

26. Kruse, P. W., McGlauchlin, L. D., and McQuistan, R. B.: Elements of Infrared Technology: Generation, Transmission, and Detection. John Wiley & Sons, Inc., 1962

27. Larach, S.: Photoelectronic Materials and Devices. D. Van Nostrand Co., Inc., 1965

28. Lasher, G. J., and Nethercot, A. H.: Theory of Optical Frequency Mixing in Bulk Photoconductors. J. Appl. Physics, Vol. 34, No. 7, July 1963, pp. 2122-2123

29. Levinstein, H.: Extrinsic Detectors. Applied Optics, Vol. 4, No. 6, June 1965, pp. 639-647

30. Lindmayer, J., and Wrigley, C. Y.: Fundamentals of Semiconductor Devices. D. Van Nostrand Co., Inc., 1965

31. Lucovsky, G., Lasser, M. E., and Emmons, R. B.: Coherent Light Detection in Solid-State Photodiodes. Proc. IEEE, Vol. 51, No. 1, Jan. 1963, pp. 166-172

32. Moreland, J. P.: Improvement of Optical Heterodyne Systems Through Spatial Filtering. Antenna Laboratory. Dept. of Elec. Engineering, The Ohio State University Research Foundation, Columbus, Ohio, Technical Report 2156-1, 10 Feb. 1966

33. Moss, T. S.: Optical Properties of Semiconductors. Butterworths, 1961

34. Oliver, B. M.: Signal-to-Noise Ratios in Photoelectric Mixing. Proc. IRE, Vol. 49, No. 12, Dec. 1961, pp. 1960-1961

35. Oliver, B. M.: Thermal and Quantum Noise. Proc. IEEE, Vol. 53, No. 5, May 1965, pp. 436-454

36. Panter, P. F.: Modulation, Noise, and Spectral Analysis. McGraw-Hill Book Co., Inc., 1965

37. Penchina, C.M., and Levinstein, H.: Measurement of Lifetimes in Photoconductors by Means of Optical Beating. Infrared Physics, Vol. 6, No. 4, Dec. 1966, pp. 173-182

38. Picus, G. S.: Far Infrared Laser Receiver Investigation. Interim Technical Report No. 3, 1 Sept. 1966 through 30 Nov. 1966. DDC Document AD 810764

39. Picus, G. S., and Buczek, C.: Far Infrared Laser Receiver Investigation. Interim Technical Report No. 4, 15 Feb. 1967 through 15 May 1967. DDC Document AD 816145

40. Plotkin, H. H.: Signal and Noise in Current Source Optical Detectors. Unpublished technical memorandum

41. Putley, E. H.: Far Infra-Red Photoconductivity. Physica Status Solidi, Vol. 6, No. 3, 1964, pp. 572-614

42. Rittner, E. S.: Electron Processes in Photoconductors. Photoconductivity Conference. John Wiley & Sons, Inc., 1956

43. Rose, A.: Concepts in Photoconductivity and Allied Problems. Interscience, 1963

44. Rosenberg, H. M.: Low Temperature Solid State Physics. Oxford University Press, 1963

45. Ross, M.: Laser Receivers. John Wiley & Sons, Inc., 1966

46. Ryvkin, S. M.: Photoelectric Effects in Semiconductors. Consultants Bureau, 1964

47. Sautter, D.: Noise in Semiconductors. Progress in Semiconductors. Vol. 4. John Wiley & Sons, Inc., 1960

48. Sawchuk, A. A.: Signal and Noise Relationships in Optical Detectors. Unpublished technical memorandum

49. Schwartz, M.: Information Transmission, Modulation, and Noise. McGraw-Hill Book Co., Inc., 1959

50. Siegman, A. E.: The Antenna Properties of Optical Heterodyne Receivers. Applied Optics, Vol. 5, No. 10, Oct. 1966, pp. 1588-1594

51. Smith, R. L.: Theory of Photoelectric Mixing at a Metal Surface. Applied Optics, Vol. 3, No. 6, June 1964, pp. 709-713

52. Sommers, H. S.: Demodulation of Low-Level Broad-Band Optical Signals with Semiconductors. Proc. IEEE, Vol. 51, No. 1, Jan. 1963, pp. 140-146

53. Sommers, H. S., and Gatchell, E. K.: BLIP Condition in Point-to-Point Optical Communication. Proc. IEEE, Vol. 55, No. 2, Feb. 1967, pp. 189-192

54. Sommers, H. S., and Gatchell, E.K.: Demodulation of Low-Level Broad-Band Optical Signals with Semiconductors. Proc. IEEE, Vol. 54, No. 11, Nov. 1966, pp. 1553-1568

55. Sommers, H. S., and Teutsch, W. B.: Demodulation of Low-Level Broad-Band Optical Signals with Semiconductors: Part II — Analysis of the Photoconductive Detector. Proc. IEEE, Vol. 52, No. 2, Feb. 1964, pp. 144-153

56. Spicer, W. E.: Relationship Between Signal-to-Noise Ratio and Threshold of Response of Infrared Photoconductors Limited by Generation-Recombination Noise. J. Appl. Physics, Vol. 30, No. 9, Sept. 1959, pp. 1381-1384

57. Teich, M. C.: Infrared Heterodyne Detection. Proc. IEEE, Vol. 56, No. 1, Jan. 1968, pp. 37-46

58. Teich, M. C., Keyes, R. J., and Kingston, R. H.: Optimum Heterodyne Detection at 10.6 Microns in Photoconductive Ge:Cu. Appl. Phys. Letters, Vol. 9, No. 10, 15 Nov. 1966, pp. 357-360

59. Van der Ziel, A.: Fluctuation Phenomena in Semiconductors. Academic Press, Inc., 1959

60. Van der Ziel, A.: Noise. Prentice-Hall, Inc., 1954

61. Van Vliet, K. M.: Noise in Semiconductors and Photoconductors. Proc. IRE, Vol. 46, No. 6, June 1958, pp. 1004-1018

62. Verie, C., and Ayas, J.: $Cd_xHg_{1-x}Te$ Infrared Photovoltaic Detectors. Appl. Phys. Letters, Vol. 10, No. 9, 1 May 1967, pp. 241-243

63. Wolfe, W. L.: Handbook of Military Infrared Technology. Office of Naval Research. Dept. of the Navy. Washington, D. C. 1965

64. Yardley, J. T., and Moore, D. B.: Response Times of Ge:Cu Infrared Detectors. Appl. Phys. Letters, Vol. 7, No. 11, 1 Dec. 1965, pp. 311-312

Appendix A

FUNDAMENTAL EQUATIONS OF PHOTOCONDUCTIVITY

There are three classes of photoconductivity: intrinsic, extrinsic, and free carrier. Intrinsic photoconductivity occurs when the absorption of a photon raises an electron from the valence band to the conduction band (creating, therefore, an electron-hole pair which increases the conductivity of the semiconductor). Extrinsic photoconductivity involves one of two possible transitions: first, an absorbed photon may raise an electron from a donor level to the conduction band or, second, an electron may be raised from the valence band to an acceptor level — leaving, therefore, a "hole" in the valence band. Free carrier photoconductivity depends upon electron transitions to higher levels within the conduction band or hole transitions deeper into the valence band.

The preceding discussion leads to the conclusion that the requirement for photon absorption is that the photon possess at least the amount of energy necessary to raise an electron to the next higher permitted energy level. This amount of energy may represent the width of the forbidden energy band, as in intrinsic photoconduction; the energy difference between a donor level and the conduction band or an acceptor level and the valence band, as in extrinsic photoconduction; or the energy difference between permitted levels in the conduction or valence bands, as in free carrier photoconductivity. The qualitative conclusions stated above may be expressed quantitatively as

$$\lambda_c \leq \frac{h\,c}{E_g} \tag{A1}$$

where λ_c is the long wavelength cutoff, h is Planck's constant, c is the velocity of light, and E_g is the energy difference across which the current carrier must be raised. Equation (A1) gives the longest wavelength that a photon may possess and still raise an electron energy by an amount E_g.

To calculate the fluctuations in current that may be induced in a photoconductor by a changing photon flux, it is necessary to write a transport equation for the majority current carrier. Since acceptor-doped germanium is most commonly used for detection of 10.6 micron radiation, the equation will be written for holes rather than electrons. The transport equation governing the behavior of free holes is

$$\frac{\partial p}{\partial t} = -\frac{p}{\tau} + g_{vt} - r_{tv} + f - \frac{1}{e}\nabla \cdot \vec{J}_h \qquad \text{(A2)}$$

where

$$\vec{J}_h = e\mu p\vec{E} - eD_h \nabla p \qquad \text{(A3)}$$

Examining the right-hand side of Equation (A2), it is seen that the first term describes the recombination rate of excess carriers. The second two terms give the rate excess carriers are produced by generation and recombination between majority carriers and trapping levels. The fourth term is the volume-density excitation rate of carriers released by the incident radiation. The fifth term accounts for diffusion effects.

If end-effects, space-charge effects, trapping (except as it affects carrier lifetime), and diffusion are ignored, Equation (A2) may be approximated, for engineering design purposes, by

$$\frac{dp}{dt} = \eta P(t) - \frac{p}{\tau} \qquad \text{(A4)}$$

where $P(t)$ is the incident photon flux, p is the hole density, η is the responsive quantum efficiency (excitations per photon), and τ is the hole lifetime. The responsive quantum efficiency may be written as

$$\eta = \frac{(1 - R)(1 - \epsilon^{-\alpha L})}{(1 - R\epsilon^{-\alpha L})} \qquad \text{(A5)}$$

where R is the reflection coefficient at the photoconductor surface, L is the dimension of the photoconductor along the direction of incident radiation, and α is the absorption coefficient. The reflection coefficient may be calculated by the relationship

$$R = \left(\frac{1 - \sqrt{K}}{1 + \sqrt{K}}\right)^2 \qquad \text{(A6)}$$

where K is the relative dielectric constant of the photoconductor.

Since Equation (A4) is simply a linear first-order differential equation, its solution is given by (ignoring an initial hole concentration)

$$p \cong \epsilon^{-t/\tau} \int \eta P(t) \epsilon^{t/\tau} \, dt \tag{A7}$$

Therefore, the photoinduced current in the photoconductor is

$$i = e G \left[\epsilon^{-t/\tau} \int \frac{\eta}{\tau} P(t) \epsilon^{t/\tau} \, dt\right] \tag{A8}$$

where

$$G = \frac{\tau}{T_r} \tag{A9}$$

and T_r is the transit time for a majority carrier. G is referred to as the photoconductive gain.

Appendix B

NOISE PHENOMENA IN PHOTOCONDUCTORS

There are five dominant noise sources which must be considered in the application of photoconductive detectors:

- Johnson noise
- Low-frequency noise
- Background noise
- Amplifier noise
- Generation-recombination noise.

The most important of these, in foreseeable communications applications, is generation-recombination noise. It will, therefore, receive the most attention.

Johnson Noise

Johnson noise, also called thermal noise, is created by thermal interactions between free electrons and vibrating ions in a conducting material. This noise is intimately related to the ordinary resistance which every photoconductor possesses. The spectral distribution of the noise extends from dc to frequencies of the order of 10^{13} Hz.[1] The mean square noise current is given by

$$\overline{i_J^2} = \frac{4 k T_p \Delta f}{R_p} \tag{B1}$$

where T_p is the temperature of the photoconductor, Δf is the electrical bandwidth, and R_p is the resistance of the photoconductor.

Low-frequency Noise

Low-frequency noise, or 1/f noise as it is sometimes called, is normally associated with the contacts on the photoconductor. This noise exhibits a spectral

[1] Schwartz, M.: Information Transmission, Modulation and Noise. McGraw-Hill Book Co., Inc., 1959, p. 214.

distribution which varies as $1/f^z$, where z has been observed to vary from approximately 0.8 to 3.0, although a value in the vicinity of unity is most common. An empirical relationship[2] may be stated as

$$\overline{i_{LF}^2} = \frac{A I^W \Delta f}{f^z} \tag{B2}$$

where A is a constant of proportionality; I is the total current flowing in the photoconductor; W is a constant associated with the particular detector, typically varying between 1.25 and 4.0 with a common value of 2.0; and Δf is the electrical bandwidth.

Amplifier Noise

The preamplifier which follows a photoconductor in most applications is not an integral part of the photoconductor, but, particularly in applications where the signal to be detected is very small, the noise generated by the amplifier may be the dominant noise power in the system. While careful design and selection of a preamplifier may lower the noise power that it introduces into the system, amplifier noise cannot be neglected in an analysis of photoconductive detection. The amplifier noise is given by

$$\overline{i_A^2} = \frac{4 k T_A \Delta f}{R_L} \tag{B3}$$

where T_A is the effective input noise temperature of the preamplifier and R_L appears because it is assumed that the preamplifier has been matched to the load resistance.

Amplifier noise is most severe in envelope detection when a liquid helium cooled detector is used with a room temperature preamplifier.

Generation-Recombination Noise

Generation-recombination noise is the predominant noise in the intermediate frequency range where most photoconductors are employed. Generation-recombination noise, or G-R noise as it is commonly referred to, is the result of

[2]Ross, M.: Laser Receivers. John Wiley & Sons, Inc., 1966, p. 58.

statistical fluctuations in the current carrier concentration. There are two equations for G-R noise which are frequently applied in the preceding report. The first of these expresses the G-R noise in terms of the dc current flowing through the photoconductor, I_o. The relationship is

$$\overline{i^2_{G-R}} = \frac{4\, e\, I_o\, G \Delta f}{1 + \omega^2 \tau^2} \tag{B4}$$

where ω is the electrical frequency to which the photoconductor must respond. In a heterodyne system, this would be the intermediate frequency. If the dc current flowing in the photoconductor is primarily due to a photon flux, as in the case of a local oscillator signal, the G-R noise can be expressed in terms of the power of that flux as

$$\overline{i^2_{G-R}} = \frac{4\, e^2\, \eta\, G^2\, \Delta f\, \overline{P}}{h\nu\,(1 + \omega^2 \tau^2)} \tag{B5}$$

Background Noise

Photons arising from other sources than the desired signal may be incident upon a photoconductor and give rise to noise currents. This noise is referred to as background noise. It is the same as the generation-recombination noise discussed in the preceding section — the distinction being in the source of the noise rather than a fundamental physical difference. The mean-squared noise current due to background radiation is, therefore, assuming a narrow optical bandwidth centered on ν,

$$\overline{i^2_B} = \frac{4\, e^2\, \eta\, G^2\, \Delta f\, \overline{P}_B}{h\nu(1 + \omega^2 \tau^2)} \tag{B6}$$

where $\overline{P_B}$ is the average background power incident upon the photoconductor.

Spectral Extent of the Various Noise Powers

Figure B1 shows the spectral distribution of the low-frequency, generation-recombination, and thermal noise. Background noise has not been included specifically, but may be considered to be included with the generation-recombination noise.

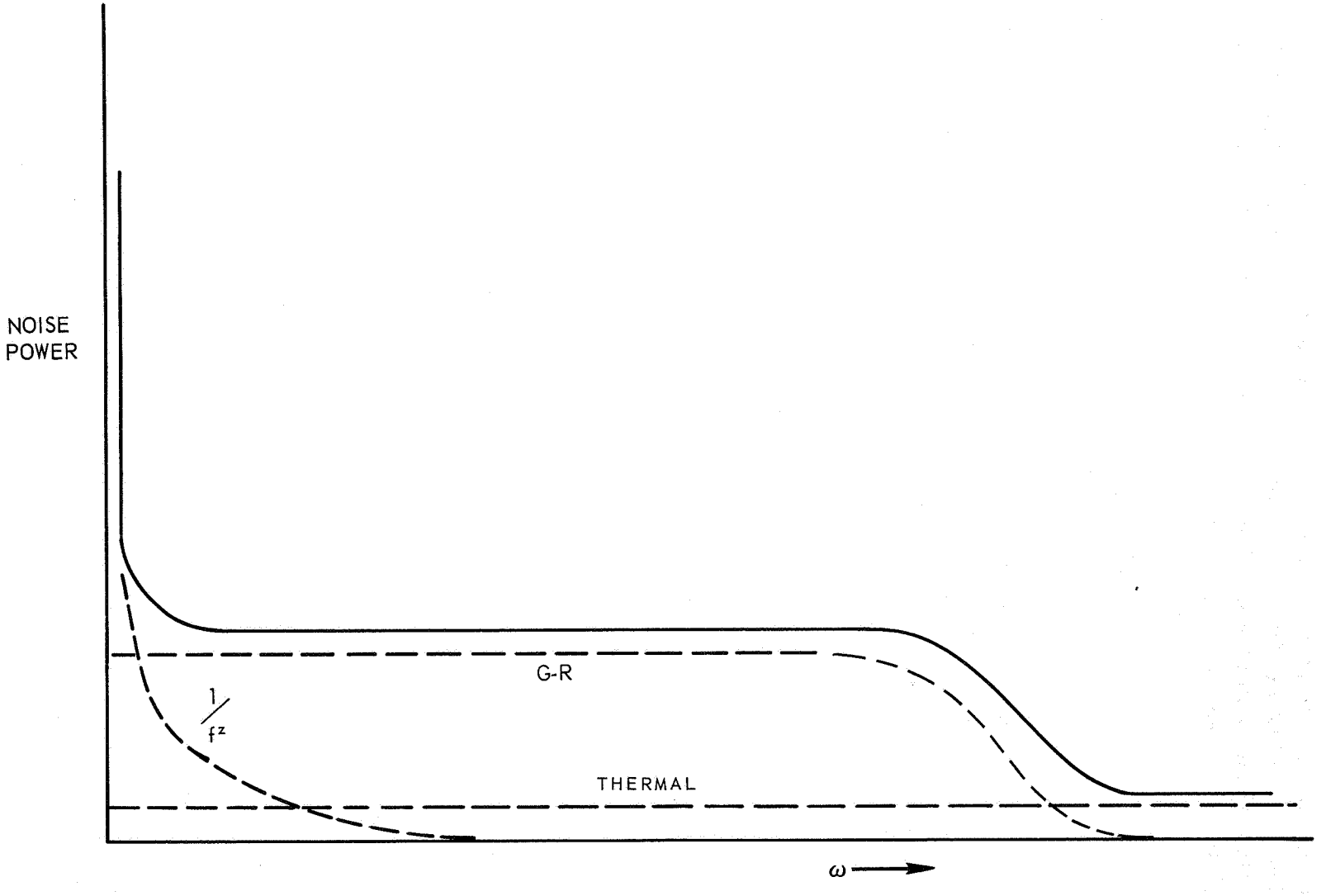

Figure B1. Spectral Distribution of Low-Frequency, Generation-Recombination, and Thermal Noise

Appendix C

REPRESENTATION OF MODULATED OPTICAL SIGNALS

The following appendix is devoted to a listing of the mathematical representations of modulated optical signals which are used in this report. Four types of amplitude modulated signals will be discussed:

- Simple amplitude modulation (AM)
- Amplitude modulation in which only the carrier and one sideband are transmitted (AMSSB)
- Amplitude modulation in which the two sidebands are transmitted but the carrier is not (AMDSB)
- Amplitude modulation in which only one sideband is transmitted and the carrier is suppressed (AMSSBSC).

Two types of angle-modulated signals will be considered:

- Phase modulation
- Frequency modulation.

Simple Amplitude Modulation (AM)

The electric field of an optical wave, amplitude modulated by a single frequency, is given by

$$\mathcal{E}_s = E_c \cos \omega_c t \, (1 + m \cos \omega_m t) \tag{C1}$$

where E_c is the peak amplitude of the optical frequency carrier, ω_c is the frequency of the optical carrier, m is the modulation index, and ω_m is the modulation frequency.

AMSSB

If the upper sideband of a simple amplitude modulated signal is suppressed, the electric field is given by

$$\mathcal{E}_s = E_c \cos \omega_c t + \frac{m E_c}{2} \cos \left[(\omega_c - \omega_m) t \right] \tag{C2}$$

AMDSB

If both sidebands are employed, but the carrier is suppressed, the electric field is

$$\mathcal{E}_s = m E_c \cos \omega_c t \cos \omega_m t . \tag{C3}$$

AMSSBSC

If the carrier and upper sideband are suppressed, the electric field is

$$\mathcal{E}_s = \frac{m E_c}{2} \cos \left[(\omega_c - \omega_m) t \right]. \tag{C4}$$

PM

There are two categories of phase modulation to be considered:

- Narrow-band phase modulation
- Wide-band modulation

The two categories are distinguished by the magnitude of the phase modulation placed upon the carrier wave. The general phase modulated wave is

$$\mathcal{E}_s = E_c \cos (\omega_c t + m_p \sin \omega_m t) \tag{C5}$$

where m_p is the phase modulation index. If $m_p \ll 1$, the system is termed narrow-band phase modulation. If m_p is not much less than one, the system is considered to be wide-band phase modulation.

FM

The electric field of a frequency modulated wave is

$$\mathcal{E}_s = E_c \cos (\omega_c t + D \sin \omega_m t) \tag{C6}$$

where

$$D \equiv \frac{2\pi f_D}{\omega_m} \tag{C7}$$

and f_D represents the peak frequency deviation of the FM signal.

Appendix D

ELEMENTARY INCOHERENT AND COHERENT DETECTION TECHNIQUES

As other photodetectors, the photoconductive detector can be employed in two distinct detection modes: incoherent detection (also known as envelope or direct detection) and coherent detection (photomixing). The object of the following paragraphs will be to clarify the distinction between the two and to discuss the relative advantages and disadvantages of each. The discussion is divided into three parts: a qualitative description of incoherent and coherent detection, an elementary quantitative discussion of each, and a comparison of the two.

Qualitative Description of Incoherent and Coherent Detection

Incoherent detection is the simpler of the two systems. A basic block diagram of incoherent detection is shown in Figure D1. When an intensity-modulated signal irradiates a photoconductor, the conductivity of the photoconductor varies in accordance with the intensity of the signal. If the photoconductor is placed in a suitable circuit (as in Figure 5), a signal is generated which may be amplified in a conventional manner until it is strong enough to serve the desired purpose.

Coherent detection, also shown in Figure D1, involves mixing the incoming signal with a separate unmodulated signal known as the local oscillator. Since the photoconductor behaves as a square-law device, the mixing of the two signals results in the production of a beat or difference frequency signal which retains the information originally carried by the modulated signal beam. Coherent detection is subdivided into homodyne and heterodyne detection. In homodyne detection the local oscillator is at the same frequency as the incoming signal's carrier frequency. In heterodyne detection the local oscillator differs by an amount called the intermediate frequency.

Elementary Quantitative Discussion of Incoherent and Coherent Detection

Signal-to-noise power ratios will now be developed for incoherent, heterodyne, and homodyne detection. The idealized case, where no frequency limitations are acknowledged in the photoconductor, will be presented.

Consider first incoherent detection. The mean signal current flowing in a photoconductor is given by

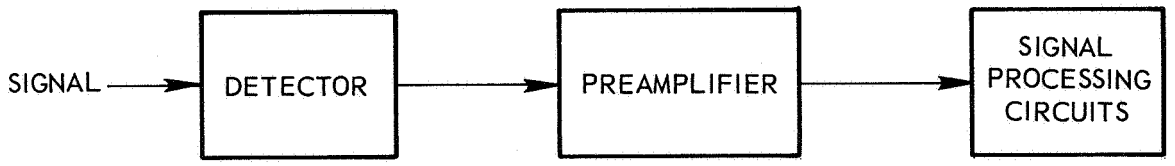

INCOHERENT DETECTION

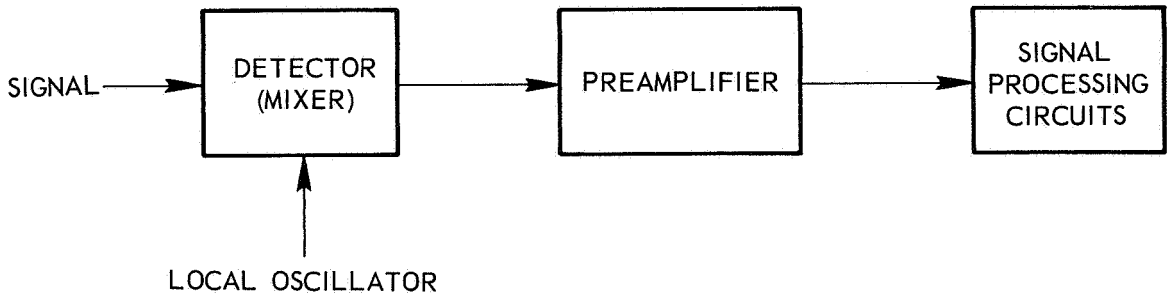

COHERENT DETECTION

Figure D1. Block Diagrams of Incoherent and Coherent Detection

$$\overline{i_s} = e\,\eta\,\frac{\overline{P_s}}{h\,\nu}\,G \tag{D1}$$

where e is the electronic charge, $\overline{P_s}$ is the average signal power incident upon the photoconductor, h is Planck's constant, ν is the signal carrier frequency, G is the photoconductive gain, and η is the responsive quantum efficiency of the detector.

Neglecting the low-frequency noise term, the signal-to-noise power ratio is given by

$$\left(\frac{S}{N}\right)_p = \frac{\left(\frac{e\,\eta\,G}{h\,\nu}\right)^2 \overline{P_s^2}}{4\,e^2\,\frac{\eta\,G^2}{h\,\nu}\,\Delta f\,(\overline{P_s} + \overline{P_B}) + \frac{4\,k\,(T_p + T_A)\,\Delta f}{R_p}} \tag{D2}$$

where $\overline{P_B}$ is the average background power, k is Boltzmann's constant, Δf is the system bandwidth, T_p is the absolute temperature of the photoconductor, T_A is the effective input noise temperature of the succeeding amplifier, and R_p is the average resistance of the photoconductor. It is assumed that the photoconductor resistance is matched to its load resistance, which is in turn matched to the input resistance of the preamplifier.

In the ideal case, the detector would be limited by the signal-induced generation-recombination noise. For that situation, the signal-to-noise power ratio becomes

$$\left(\frac{S}{N}\right)_p = \frac{\eta \overline{P_s}}{4 h \nu \Delta f} . \tag{D3}$$

It should be noted that Equation (D3) is 3 db worse than the equation obtained for photoelectric detection. Shot noise in the photoelectric case is a factor of two less because it is related only to a random generation process; generation-recombination noise has its roots in both a random generation and recombination process. It is convenient to speak of a noise-equivalent-power (NEP) as the power, for a one Hz bandwidth and a unity quantum efficiency, at which the signal-to-noise power ratio is unity. Rearranging Equation (D3) and substituting gives

$$NEP = 4 h \nu \tag{D4}$$

For the CO_2 laser, this corresponds to a limiting value of nominally 5×10^{-20} watt. It should be noted that this value is a theoretical ideal which is not realizable in practice. The noise terms that were neglected limit the value to the order of 10^{-13} watt.

A similar expression will now be developed for heterodyne detection. In this case the total signal current is given by

$$\overline{i_T} = \frac{e \eta G}{h \nu} \overline{P_T} \tag{D5}$$

where

$$\overline{P_T} = \sqrt{\frac{\epsilon}{\mu}} \overline{\left[E_c \cos \omega_c t \, (1 + m \cos \omega_m t) + E_L \cos (\omega_L t + \phi)\right]^2} , \tag{D6}$$

E_c is the peak carrier E-field, ω_c is the carrier frequency, m is the modulation index, E_L is the peak local oscillator E-field, ω_L is the local oscillator frequency, and ϕ is an arbitrary phase angle. The bar over the squared quantity indicates that the mean value must be found.

After taking the mean value and selecting only the signal component of the expression, the mean-squared signal current is found to be

$$\overline{i_s^2} = \left(\frac{e\,\eta\,G}{h\,\nu}\right)^2 2\,\overline{P_{LO}}\,\overline{P_s} \tag{D7}$$

where $\overline{P_{LO}}$ is the mean local oscillator power given by

$$\overline{P_{LO}} = \sqrt{\frac{\epsilon}{\mu}}\,\frac{E_L^2}{2} \tag{D8}$$

and $\overline{P_s}$ is the mean signal power given by

$$\overline{P_s} = \sqrt{\frac{\epsilon}{\mu}}\,\frac{m^2 E_c^2}{4} \tag{D9}$$

Therefore, the signal-to-noise power ratio is

$$\left(\frac{S}{N}\right)_p = \frac{\left(\frac{e\,\eta\,G}{h\,\nu}\right)^2 2\,\overline{P_{LO}}\,\overline{P_s}}{4\,\frac{e^2\,\eta\,G^2}{h\,\nu}\,\Delta f\,(\overline{P_{LO}} + \overline{P_s} + \overline{P_B}) + \frac{4\,k\,(T_p + T_A)\,\Delta f}{R_p}} \tag{D10}$$

If the local oscillator power is increased until it dominates all other terms in the denominator,

$$\left(\frac{S}{N}\right)_p = \frac{\eta\,\overline{P_s}}{2\,h\,\nu\,\Delta f} \tag{D11}$$

It is seen that the ideal signal-to-noise power ratio is a factor of two better than that for the incoherent detection case. There is, however, a far more significant difference. Note that to obtain the ideal case in incoherent detection it was necessary to assume that all noise terms other than the signal generation-recombination noise were negligible. Contrast this with the attainment of the ideal case for heterodyne detection by simply increasing the local oscillator power. This makes the ideal case far more attainable in heterodyne detection. The NEP for the ideal heterodyne detection system is

$$\text{NEP} = 2h\nu \tag{D12}$$

or nominally 2.5×10^{-20} watt for the 10.6 micron system.

If the carrier and local oscillator are at the same frequency, homodyne detection results. The mean-squared signal current becomes

$$\overline{i_s^2} = \left(\frac{e\eta G}{h\nu}\right)^2 4\,\overline{P_{LO}}\,\overline{P_s}\cos^2\phi \tag{D13}$$

where ϕ is the phase difference between the carrier and local oscillator and all other symbols have the same meaning as previously. The signal-to-noise power ratio is

$$\left(\frac{S}{N}\right)_p = \frac{\left(\frac{e\eta G}{h\nu}\right)^2 4\,\overline{P_{LO}}\,\overline{P_s}\cos^2\phi}{\frac{4e^2\eta G^2}{h\nu}\Delta f\,(\overline{P_{LO}} + \overline{P_s} + \overline{P_B}) + \frac{4k(T_p + T_A)\Delta f}{R_p}} \tag{D14}$$

If the local oscillator power is increased until it dominates all other noise sources,

$$\left(\frac{S}{N}\right)_p = \frac{\eta\,\overline{P_s}}{h\nu\,\Delta f}\cos^2\phi \tag{D15}$$

Therefore, it can be seen that, provided ϕ can be nulled (and maintained in a nulled condition — which may be no easy technological problem), homodyne

detection can be a factor of two better than heterodyne detection. If ϕ must be considered random, $\cos^2 \phi$ must be given the value ½ and heterodyne and homodyne detection are equivalent. Assuming that ϕ is nulled,

$$NEP = h\nu \tag{D16}$$

or approximately 1.25×10^{-20} watt for 10.6 microns.

Comparison of Incoherent and Coherent Detection

Incoherent detection has four major advantages over coherent detection: first, the mechanical alignment is much less critical; second, the system is far less susceptible to disruption by mechanical vibrations; third, disturbances of the spatial or temporal coherence of the signal beam, as might be produced by the atmosphere or imperfect optical components, do not prevent or seriously impede reception; and, finally, no local oscillator is required.

Coherent detection has two major advantages: first, because of the capability to discriminate against background noise and other noise sources, coherent detection may be as much as six orders of magnitude more sensitive than incoherent detection and, second, it is possible to receive angle-modulated signals (PM and FM) with coherent detection, but not with incoherent detection.

Appendix E

DETAILED DERIVATION OF SIGNAL-TO-NOISE POWER RATIO FOR HETERODYNE DETECTION OF SIMPLE AM SIGNAL

In the following appendix a detailed derivation of Equation (4) of this report is given. The purpose of this appendix is not only to illustrate how that particular equation was arrived at, but also to give an example of the derivations which led to all of the signal-to-noise power ratios given in this report. The pattern of each derivation was nearly identical to the one given below.

The total incident E-field irradiating the detector is the sum of the signal and local oscillator signals and is given by

$$\mathcal{E}_R = E_c (1 + m \cos \omega_m t) \cos \omega_c t + E_L \cos (\omega_L t + \phi) \tag{E1}$$

Perfect alignment of signal and local oscillator beams has been assumed. A photoconductor responds to the power of the incident radiation. The mean power contained in the signal represented by Equation (E1) is, in terms of a photon flux,

$$\overline{P_R} = \sqrt{\frac{\epsilon}{\mu}} \frac{\overline{\mathcal{E}_R^2}}{h\nu} \tag{E2}$$

Squaring the field represented by Equation (E1) gives, after ignoring terms involving E_c^2,

$$\mathcal{E}_R^2 = E_L^2 \cos^2 (\omega_L t + \phi) + 2 E_L E_c (1 + m \cos \omega_m t) \cos \omega_c t \cos (\omega_L t + \phi) \tag{E3}$$

Assuming that ϕ is zero and expanding the final product of two cosines leads to

$$\mathcal{E}_R^2 = E_L^2 \cos^2 \omega_L t + E_L E_c (1 + m \cos \omega_m t) \left\{ \cos \left[(\omega_L + \omega_c) t \right] + \cos \left[(\omega_L - \omega_c) t \right] \right\} \tag{E4}$$

Since the detector cannot respond to frequencies as high as $\omega_L + \omega_c$,

$$\mathcal{E}_R^2 = E_L^2 \cos^2 \omega_L t + E_L E_c (1 + m \cos \omega_m t) \cos \omega_{IF} t \qquad \text{(E5)}$$

where

$$\omega_{IF} = \omega_L - \omega_c . \qquad \text{(E6)}$$

Once again expanding the product of two cosine terms,

$$\mathcal{E}_R^2 = E_L^2 \cos^2 \omega_L t + E_L E_c \cos \omega_{IF} t$$

$$+ \frac{m E_L E_c}{2} \left\{ \cos \left[(\omega_{IF} + \omega_m) t \right] + \cos \left[(\omega_{IF} - \omega_m) t \right] \right\} \qquad \text{(E7)}$$

Averaging over a period, T, such that

$$\frac{2\pi}{\omega_c} << T << \frac{2\pi}{\omega_{IF} \pm \omega_m}$$

gives

$$\overline{\mathcal{E}_R^2} = \frac{E_L^2}{2} + E_L E_c \cos \omega_{IF} t$$

$$+ \frac{m E_L E_c}{2} \left\{ \cos \left[(\omega_{IF} + \omega_m) t \right] + \cos \left[(\omega_{IF} - \omega_m) t \right] \right\} \qquad \text{(E8)}$$

Substituting into Equation (1) gives

$$i = \frac{e\eta G}{h\nu}\sqrt{\frac{\epsilon}{\mu}}\ \frac{\epsilon^{-t/\tau}}{\tau}\int \mathcal{E}_R^2\,\epsilon^{t/\tau}\,dt$$

$$= \frac{e\eta G}{h\nu}\sqrt{\frac{\epsilon}{\mu}}\left[\frac{E_L^2}{2} + \frac{E_L E_c \cos(\omega_{IF} t + \xi_0)}{\sqrt{1 + (\omega_{IF}\tau)^2}}\right]$$

(E9)

$$+ \frac{e\eta G}{h\nu}\sqrt{\frac{\epsilon}{\mu}}\ \frac{m E_L E_c}{2}\left\{\frac{\cos\left[(\omega_{IF} + \omega_m) t + \xi_1\right]}{\sqrt{1 + \left[(\omega_{IF} + \omega_m)\tau\right]^2}} + \frac{\cos\left[(\omega_{IF} - \omega_m) t + \xi_2\right]}{\sqrt{1 + \left[(\omega_{IF} - \omega_m)\tau\right]^2}}\right\}$$

where

$$\xi_0 = \mathrm{Tan}^{-1}(-\omega_{IF}\tau),$$

$$\xi_1 = \mathrm{Tan}^{-1}\left[-(\omega_{IF} + \omega_m)\tau\right],$$

and

$$\xi_2 = \mathrm{Tan}^{-1}\left[-(\omega_{IF} - \omega_m)\tau\right].$$

Taking the mean-squared value of the desired signal component of Equation (E9) gives, provided that $\omega_{IF} >> \omega_m$,

$$\overline{i_s^2} = \left(\frac{e\eta G}{h\nu}\right)^2 \left(2\sqrt{\frac{\epsilon}{\mu}}\ \frac{E_L^2}{2}\right)\left(\sqrt{\frac{\epsilon}{\mu}}\ \frac{m^2 E_c^2}{4}\right)(1 + \omega_{IF}^2\tau^2)^{-1}$$

$$= \left(\frac{e\eta G}{h\nu}\right)^2 2\,\overline{P_{LO}}\,\overline{P_s}\,(1 + \omega_{IF}^2\tau^2)^{-1}. \qquad \text{(E10)}$$

Therefore, the signal-to-noise power ratio is

$$\left(\frac{S}{N}\right)_p = \frac{\left(\frac{e\eta G}{h\nu}\right)^2 2\,\overline{P_{LO}}\,\overline{P_s}\,(1+\omega_{IF}^2\tau^2)^{-1}}{\frac{4e^2\eta G^2}{h\nu}\,\frac{\Delta f\,(\overline{P_{LO}}+\overline{P_s}+\overline{P_B})}{1+\omega_{IF}^2\tau^2}+\frac{4k(T_p+T_A)\Delta f}{R_p}} \qquad \text{(E11)}$$

Assuming that $\overline{P_{LO}} \gg \overline{P_s}$ or $\overline{P_B}$,

$$\left(\frac{S}{N}\right)_p = \frac{\left(\frac{e\eta G}{h\nu}\right)^2 2\,\overline{P_{LO}}\,\overline{P_s}\,(1+\omega_{IF}^2\tau^2)^{-1}}{\frac{4e^2\eta G^2\Delta f}{h\nu}\,\frac{\overline{P_{LO}}}{1+\omega_{IF}^2\tau^2}+\frac{4k(T_p+T_A)\Delta f}{R_p}}$$

$$= \frac{\eta\overline{P_s}}{2h\nu\Delta f}\left[1+\frac{k(T_p+T_A)(1+\omega_{IF}^2\tau^2)}{eV_pG}\right]^{-1} \qquad \text{(E12)}$$

Appendix F

DERIVATION OF MAJORITY CARRIER MOBILITY EQUATION

This appendix is devoted to a detailed derivation of Equation (33). Differentiating the standard voltage divider relationship gives

$$\frac{dV_s}{d\sigma} = -\frac{R_L V}{(R_p + R_L)^2} \frac{L}{\sigma^2 D W} \tag{F1}$$

or

$$\Delta V_s \cong -\frac{R_L V}{(R_p + R_L)^2} \frac{L}{\sigma^2 D W} \Delta\sigma \tag{F2}$$

where σ is the conductivity of the photoconductor and R_p is its resistance. It is clear that (F2) will only give reasonable answers if the change in conductivity is small. The change in conductivity can be expressed as

$$\Delta\sigma = (\Delta p)\, e\, \mu = (\Delta f_e)\, \tau\, e\, \mu \tag{F3}$$

where Δp is the change in carrier density, μ is the carrier mobility, and Δf_e is the change in the excitation rate per unit volume. Therefore,

$$\Delta V_s = -\frac{R_L V}{(R_p + R_L)^2} \frac{L (\Delta f_e)\, \tau\, e\, \mu}{(p\, e\, \mu)^2 D W}$$

$$= -\frac{R_L R_p V \eta P_s \tau}{(R_L + R_p)^2\, p\, h\, \nu} \tag{F4}$$

since

$$\Delta f_e = \frac{\eta \Delta P_s}{h \nu L D W} \tag{F5}$$

and

$$R_p = \frac{L}{p e \mu D W} . \tag{F6}$$

Similarly, using Equation (F6), the total change in the number of generated carriers is

$$N = \frac{\sigma}{e \mu} L D W = \frac{1}{e \mu} \frac{L^2}{R_p} . \tag{F7}$$

Therefore,

$$p = \frac{N}{L D W} = \frac{L}{e \mu R_p D W} . \tag{F8}$$

Solving (F4) for p, and equating it to the right side of (F8), and solving the resulting equation of μ gives

$$\mu = \frac{L (R_L + R_p)^2 h \nu}{R_L R_p^2 V e D W \eta \tau} \frac{\Delta V_s}{\Delta P_s} . \tag{F9}$$